Upregulated Ca²⁺ release from the endoplasmic reticulum leads to impaired presynaptic function in familial Alzheimer's disease

Temitope Adeoye [1], Syed I Shah [1], Angelo Demuro [2], David A Rabson [1], and Ghanim Ullah [1,*]

[1] Department of Physics, University of South Florida, Tampa, FL 33620; tadeoye@usf.edu; syedislam-udd@usf.edu; rabson@usf.edu; gullah@usf.edu
[2] Department of Neurobiology and Behavior University of California, Irvine, CA 92697; ademuro@uci.edu
* Correspondence: gullah@usf.edu;

Abstract: Neurotransmitter release from presynaptic terminals is primarily regulated by rapid Ca²⁺ influx through membrane-resident voltage-gated Ca²⁺ channels (VGCCs). Also, accumulating evidence indicates that the endoplasmic reticulum (ER) is extensively present in axonal terminals of neurons and plays a modulatory role in synaptic transmission by regulating Ca²⁺ levels. Familial Alzheimer's disease (FAD) is marked by enhanced Ca²⁺ release from the ER and downregulation of Ca²⁺ buffering proteins. However, the precise consequence of impaired Ca²⁺ signaling within the vicinity of VGCCs (active zone (AZ)) on exocytosis is poorly understood. Here, we perform in-silico experiments of intracellular Ca²⁺ signaling and exocytosis in a detailed biophysical model of hippocampal synapses to investigate the effect of aberrant Ca²⁺ signaling on neurotransmitter release in FAD. Our model predicts that enhanced Ca²⁺ release from the ER increases the probability of neurotransmitter release in FAD. Moreover, over very short timescales (30-60 msec), the model exhibits activity-dependent and enhanced short-term plasticity in FAD, indicating neuronal hyperactivity— a hallmark of the disease. Similar to previous observations in AD animal models, our model reveals that during prolonged stimulation (~450 msec), pathological Ca²⁺ signaling increases depression and desynchronization with stimulus, causing affected synapses to operate unreliably. Overall, our work provides direct evidence in support of a crucial role played by altered Ca²⁺ homeostasis mediated by intracellular stores in FAD.

1. Introduction

Alzheimer's disease (AD) is the most common and burdensome of the late-onset degenerative dementias: the world Alzheimer's report estimated a global prevalence of over 50 million worldwide, a number expected to triple by 2050 [1, 2]. AD manifests as progressive memory impairment initially and faster rate of cognitive decline and neurodegeneration in later stages, along with behavioral and physiological manifestations [3]. Despite the convoluted etiology of AD, experimental and theoretical investigation suggests that synapses are the primary targets in the early stage of the disease [4]. Histologically, the AD brain is marked by extracellular deposition of senile beta-amyloid (Aβ) plaques— in early-onset FAD, this accumulation has been traced to abnormalities in the genes encoding amyloid precursor protein (APP) or intramembrane protease presenilin 1 and 2 (PS1, PS2). While rare (5% of AD cases), this form of Alzheimer's disease holds an estimated heritability over 90% [5]. These abnormalities are accompanied by intracellular

accumulation of neurofibrillary tangles (NFTs)—composed of hyperphosphorylated tau proteins (pTau)—that litter the cerebral and hippocampal cortices [6—9]. Although the exact mechanism is still being debated, numerous experimental studies implicate elevated intracellular Ca^{2+} levels as one of the main mechanisms underlying $A\beta$ toxicity [10, 11]. These studies show that the AD brain is surfeit with dysregulation of Ca^{2+} signaling pathways [10—13], motivating researchers to propose the Ca^{2+} hypothesis of AD and aging [17]. Indeed, it has been shown that both intra- and extracellular $A\beta$ oligomers and FADcausing mutations in presenilin result in enhanced Ca^{2+} release from the ER through inositol (1, 4, 5)-triphosphate (IP3) receptors (IP_3Rs) and/or ryanodine receptors (RyRs) [10—22]. This upregulated Ca^{2+} release can contribute to aberrant plasticity and functional disruption of neuronal networks [11, 23].

Intracellular Ca^{2+} is an important second messenger, regulating a multitude of neuronal functions, including neurotransmitter release. Synaptic function at nerve terminals is tightly coupled to intracellular Ca^{2+} concentration ($[Ca^{2+}]$), as Ca^{2+} primarily regulates the biological machinery responsible for exocytosis and short-term plasticity [24, 25]. The precise temporal control of synaptic transmission by Ca^{2+} is achieved via local signal transduction mechanisms that aim to regulate Ca^{2+} excitability at the axonal bouton. Voltage-gated Ca^{2+} channels (VGCCs) are the primary mediators of the transduction of depolarization-induced Ca^{2+} transients into neurotransmitter release. Furthermore, Ca^{2+} influx through VGCCs leads to physiological events that alter plasma membrane functions underpinning synaptic plasticity, protein expression, spine maintenance, and regulation of excitability in excitatory synapses [26, 27]. Likewise, investigations of the Ca^{2+}-dependence of vesicular release have highlighted the role of intracellular stores in Ca^{2+} handling and spontaneous exocytosis [28, 29]. Thus, the close association between these Ca^{2+} pathways, their effect on numerous neuronal processes, and their high sensitivity to pathological perturbations makes it especially valuable to elucidate the exact nature of the coupling.

Extensive evidence supports the presence of the ER in the nerve terminal of CA3 pyramidal neurons [23, 28—32]. In neurons, activation of Ca^{2+}-sensitive channels like IP_3Rs and RyRs triggers the release of Ca^{2+} from the ER. Opening of IP_3Rs primarily depends on Ca^{2+} and IP_3. To achieve this, glutamate released into the synaptic cleft elicits the production of IP_3 by the activation of membrane-bound metabotropic glutamate receptors (mGLuRs). RyRs activation, on the other hand, is largely controlled by cytosolic $[Ca^{2+}]$. This specialized cascade underscores the importance of IP_3Rs and RyRs in the regulation of the Ca^{2+} induced Ca^{2+} release (CICR) mechanism of the ER. Previous works have shown that CICR is necessary for ER stores to adequately influence spontaneous vesicle release and homosynaptic plasticity [28, 33]. Indeed, in vitro studies confirm that properly sensitized CICR is necessary for normal synaptic function, whereas aberrant CICR underlies presynaptic impairment associated with AD [34—37]. Despite this evidence, the precise role of ER Ca^{2+} handling in action potential (AP)-evoked presynaptic Ca^{2+} dynamics and its downstream effect on presynaptic neuronal processes remain unclear [28, 34, 35, 37].

Information encoding at the CA3 to CA1 synapses in the hippocampus, which is crucial for learning and memory storage, relies on the spatiotemporal organization of Ca^{2+} events leading up to synaptic transmission [38]. AP arrival at the nerve terminal activates VGCCs, leading to high-amplitude, short-lived Ca^{2+} influx events into the AZ. Coupled with this specialized pathway, Ca^{2+} sensors initiate a heterogeneous fusion of neurotransmitter vesicles with the plasma membrane that often culminates in either fast synchronous or slow asynchronous release. Neuronal communication primarily relies on the synchronous mode of exocytosis, which is regulated by synaptotagmin-1 (Syt1) sensors with low Ca^{2+} affinity and rapid kinetics that are critical for the exquisite temporal precision of vesicle fusion that characterizes synaptic transmission at most CA3-CA1 terminals [39—41]. Such a high degree of synchrony is in part achieved by the steep dose dependence of evoked release on the short-lived Ca^{2+} transients constrained to micro- or nanodomains

within the vicinity of VGCCs [24, 42]. A global buildup of [Ca²⁺], on the other hand, accelerates the recruitment of release-ready vesicles, controlling the degree of synaptic plasticity [43]. Thus, changes in Ca²⁺ signals at the local or global scale are expected to disrupt synaptic transmission and plasticity. Consistent with this assertion, experimental manipulations that perturb evoked Ca²⁺ influx alter the contribution of the synchronous mode of release to overall exocytosis and compromise synaptic plasticity [44—46]. These findings highlight the need for a thorough investigation of the potential link between impaired synaptic function and disrupted Ca²⁺ homeostasis in AD.

In this study, we incorporate findings from extensive experimental and computational studies to develop a detailed biophysical model of Ca²⁺-driven exocytosis at the CA3 presynaptic terminal. The model accounts for the observed Ca²⁺ and IP₃ signaling pathways necessary for intracellular Ca²⁺ regulation and integrates the elaborate kinetics of neurotransmitter release—vesicle docking, mobilization, priming, and fusion—aided by distinct Ca²⁺ sensors. We reproduced crucial statistics of both Ca²⁺ and release events reported at small excitatory synapses, such as transient timescale, amplitude, and decay time. By developing a mathematical framework for coupling the Ca²⁺ domains surrounding the ER and AZ, we study how FAD-associated pathological Ca²⁺ release from the ER disrupts presynaptic neurotransmitter release rates and consequently alter synaptic plasticity and facilitation at affected synapses. Overall, our work provides novel insights on the pathologic role of aberrant neuronal Ca²⁺ handling on glutamate release and the downstream effects on synaptic dysfunction and cognitive decline observed in FAD. We address the limitations of this model, noting that the inclusion of differential enrichment of VGCC subtypes, mitochondrial function, Ca²⁺ buffers, and RyRs activity in future extensions of the current work will provide a comprehensive computational framework that can be used to investigate key cellular mechanisms and processes, which in turn can be targeted for reversing presynaptic impairment in FAD.

2. Materials and Methods

2.1. Calcium model

Building on extensive literature, we capture intracellular Ca²⁺ dynamics by first developing a compartmental model of a hippocampal CA3 axonal bouton, which includes main fluxes that invade the bulk cytosol as well as regulatory mechanisms present in the ER [47—50] (Fig. 1). Our canonical synaptic bouton is modelled as a sphere with fixed volume V_{bouton} = 0.122 μm^3, in agreement with findings from ultrastructural analysis of hippocampal synapses [51, 52]. We consider an average of 1.3 AZs in small hippocampal boutons implemented in a spherical AZ (with area = 0.04 μm^2) [51, 52]. Although we assume a well-mixed cytoplasm, we next incorporate two microdomains of sharp Ca²⁺ transients produced by clusters of IP₃Rs and VGCCs proximal to the ER and plasma membrane respectively. Because the VGCCs (P/Q-type Cav2.1 channels) implemented here are spatially distributed in small clusters within the AZ, we implemented a characteristic 25 nm cluster [52, 53]. To account for the spatial extent of the Ca²⁺ domain in the vicinity of the VGCCs cluster, we use the findings in cortical pyramidal terminals that show that low mM concentrations of the slow Ca²⁺ buffer ethylene glycol tetra-acetic acid potently attenuates transmitter release [27, 54, 55] for guidance. We consider a cytosol-to-VGCCs microdomain ratio of 60, assuming a domain of elevated [Ca²⁺] that extends over more than 100 nm [27, 56]. As a result of these considerations, the Ca²⁺ dynamics in the respective compartments as well as the entire bouton ($[Ca_{total}^{2+}]$) is described by four coupled non-linear ODEs (Eqs. 1-4). Table 1 defines the fluxes (J) in terms of various Ca²⁺ concentrations, along with volume fractions. The parameters used are listed in Tables 2 and 3. IP₃ is a critical second messenger to Ca²⁺ The pathways for its metabolism are succinctly described in Eq. (5) [57, 58], with further details in Table 4. Inhomogeneity of ligands persists

throughout the bouton; however, we assume spatially homogenous compartments, and
only track temporal evolution of ligands.

$$\frac{d}{dt}[Ca_{cyt}^{2+}] = J_{in} + J_{IPR-diff} - J_{PMCA} + J_{ER-leak} + J_{VGCC-diff} - J_{SERCA} \quad (1)$$
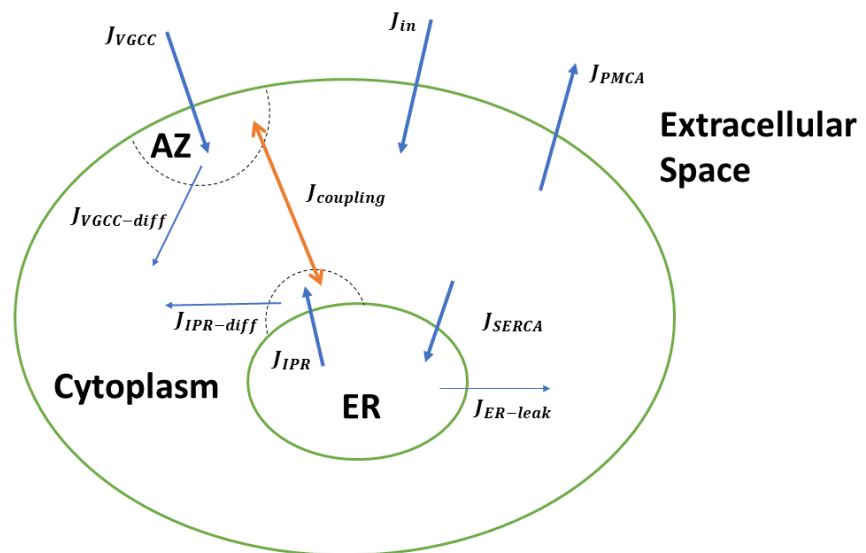
$$\frac{d}{dt}[Ca_{IPR_n}^{2+}] = \delta_1\left(J_{IPR} - J_{IPR-diff}\right) + J_{coupling} \quad (2)$$

$$\frac{d}{dt}[Ca_{AZ}^{2+}] = \delta_3\left(J_{VGCC} - J_{VGCC-diff}\right) - \frac{1}{\delta_1}J_{coupling} \quad (3)$$

$$\frac{d}{dt}[Ca_{total}^{2+}] = J_{in} - J_{PMCA} + J_{VGCC} \quad (4)$$

$$\frac{d}{dt}[IP_3] = \frac{1}{\tau_{IP_3}}\left(J_{PLC} - J_{deg}\right) \quad (5)$$

where $[Ca_{cyt}^{2+}]$ is the Ca^{2+} concentration in the cytosol, $[Ca_{IPR_n}^{2+}]$ is the Ca^{2+} concentration
in the microdomain surrounding the IP$_3$Rs, and $[Ca_{AZ}^{2+}]$ represents the Ca^{2+} concentration
surrounding the small cluster of VGCCs in the AZ.

Figure 1. Schematic of the overall multi-compartmental Ca^{2+} model. The arrowheads show the direction of the fluxes involved and the dotted half circles signify the Ca^{2+} domains around the IP$_3$Rs
and VGCCs clusters.

Table 1. Ca^{2+} fluxes in the model.

Flux (reference)	Equation
Basal leak and R/SOCC [49, 50]	$J_{in} = J_{leakin} + V_{leakin}IP_3$
Ca2+ diffusion from the IP$_3$R cluster [47]	$J_{IPR-diff} = k_{IPR-diff}\left(Ca_{IPR_n}^{2+} - Ca_{cyt}^{2+}\right)$

PMCA [47]	$J_{PMCA} = V_{PMCA} \dfrac{\left(Ca_{cyt}^{2+}\right)^n}{\left(Ca_{cyt}^{2+}\right)^n + K_{PMCA}{}^n}$
SERCA [47]	$J_{SERCA} = V_{SERCA} \dfrac{\left(Ca_{cyt}^{2+}\right)^n}{\left(Ca_{cyt}^{2+}\right)^n + K_{SERCA}{}^n}$
ER-leak [47]	$J_{ER-leak} = k_{ER-leak}\left(Ca_{ER}^{2+} - Ca_{cyt}^{2+}\right)$
IP₃ Receptor [47]	$J_{IPR} = k_{IPR}P_o\left(Ca_{ER}^{2+} - Ca_{IPR_n}^{2+}\right)$ $P_o = N_{open}/N_{IP_3R}$
Ca²⁺ diffusion from the VGCC cluster	$J_{VGCC-diff} = k_{VGCC-diff}\left(Ca_{AZ}^{2+} - Ca_{cyt}^{2+}\right)$
ER—AZ Coupling	$J_{coupling} = V_c \dfrac{\left(Ca_{AZ}^{2+2} - \bar{k}\left(Ca_{IP_3R_n}^{2+}{}^2\right)\right)}{Ca_{AZ}^{2+2} - K_c{}^2}$
VGCC [53]	$J_{VGCC} = \dfrac{-I_{Ca^{2+}}}{zFV_{cell}}$ $I_{Ca^{2+}} = channel\ density \cdot cluster\ area \cdot I_s$ $I_s = gP_o(V - E_{Ca^{2+}}),\ P_o = N_{open}/N_{VGCC}$ $channel\ density = \dfrac{N_{VGCC}}{(AZ_{area} \cdot N_{AZ})}$

170

Table 2. Parameter values for the Ca²⁺ dynamics.

171

Category	Parameters	Description	Value/Units	Notes
Cellular	J_{leakin}	Plasma membrane leak influx	0.03115 µM·ms⁻¹	From [47]
	V_{leakin}	R/SOCC flux coefficient	0.2 ms⁻¹	From [47]
	$k_{IPR-diff}$	$Ca_{IP_3R_n}^{2+}$ diffusional flux coefficient	10 ms⁻¹	From [47]
	k_{IPR}	IP₃R flux coefficient	5 ms⁻¹	Modified From [47]
	N_{IPR}	Total number of IP₃R channels	10	
	$k_{ER-leak}$	ER-leak flux coefficient	0.0022 ms⁻¹	Modified From [47]
PMCA	V_{PMCA}	Maximum capacity of PMCA	3.195 µM·ms⁻¹	Modified From [47]
	K_{PMCA}	Half activation PMCA constant	0.5 µM	From [47]
	n_P	Hill coefficient of PMCA	2	From [47]
SERCA	V_{SERCA}	Maximum capacity of SERCA	10 µM·ms⁻¹	From [47]
	K_{SERCA}	Half maximal activation SERCA	0.26 µM	From [47]
	n_S	Hill coefficient of SERCA	1.75	From [47]
VGCC and Coupling	$k_{VGCC-diff}$	Ca_{AZ}^{2+} diffusional flux coefficient	0.071 ms⁻¹	
	V_{cell}	Terminal volume	1.22×10-6 L	Modified from [53]
	cluster area	Area of VGCC cluster	0.001963 µm²	Modified from [53]
	AZ_{area}	Active zone area	0.04 µm2	Modified from [51, 53]
	N_{AZ}	Active zone number	1.3	Modified from [53]
	V_c	Maximum capacity of transfer component	118 µM·ms⁻¹	
	$\bar{k}$	Concentrating power of the transfer components.	High coupling: 15 µM Low coupling: 5 µM	
	K_c	Half-maximal transfer rate	High coupling: 10 µM Low coupling: 20 µM	

Table 3. Additional parameters used in the Ca²⁺ dynamics.

Parameter	Value / Units	Notes
Resting cytosol $[Ca^{2+}_{cyt}]$	0.1 μM	[58]
Resting AZ $[Ca^{2+}_{AZ}]$	0.05 μM	[53]
Resting Total $[Ca^{2+}_{total}]$	56 μM	
Resting $[IP_3]$	0.1 μM	[58]
Extracellular $[Ca^{2+}_{ext}]$	2.0 mM	[53]
δ_1	100	Cytoplasmic to ER microdomain volume ratio [47]
δ_2	10	Cytoplasmic to ER volume ratio [47]
δ_3	60	Cytoplasmic to VGCC microdomain volume ratio

The Ca²⁺ concentration in the ER is given by $[Ca^{2+}_{ER}] = \delta_2\big(Ca^{2+}_{total} - Ca^{2+}_{cyt} + Ca^{2+}_{IPR_n}/\delta_1 - Ca^{2+}_{AZ}\big)$. δ_1, δ_2, and δ_3 represent the volume ratios of the intracellular compartments and are explained in Table 3. Fluxes in our model were selected to account for the essential regulating components of intracellular Ca²⁺ signaling. J_{in} represents the Ca²⁺ entry through plasma membrane channels such as store operated Ca²⁺ channels (SOCC) and basal plasma membrane leak. J_{IPR} represents release from the ER through IP₃Rs, whereas Ca²⁺ diffusion from the microdomain around IP₃Rs cluster to the bulk cytosol is modelled by $J_{IPR-diff}$. Likewise, $J_{VGCC-diff}$ and J_{VGCC} are included to account for Ca²⁺ diffusion from the AZ to the bulk cytoplasm and influx through VGCCs respectively. Ca²⁺ efflux from the intracellular compartment by plasma membrane Ca²⁺ ATPase (PMCA) is captured by J_{PMCA}, and $J_{ER-leak}$ is the Ca²⁺ leak from the ER. Sequestering of Ca²⁺ from the cytoplasm into the ER through Sarco/Endoplasmic Reticulum Ca²⁺ ATPase (SERCA) is represented by J_{SERCA}.

To investigate the effect of altered ER Ca²⁺ handling on vesicular fusion situated in the AZ, we incorporate a flux ($J_{coupling}$) intended to mimic the close association of the ER with the nerve terminal of CA3 pyramidal neurons [30—32]. Based on evidence of the existence of a feedback loop between synaptic function and ER Ca²⁺ content, we build a bidirectional model of Ca²⁺ exchange. We assume a simple transfer of Ca²⁺ between the two microdomains, potentially mediated by Ca²⁺ buffering and enzymatic proteins. This coupling is modelled by an equation analogous to bidirectional models of SERCA flux (Eq. 6) [50], which where V_c is the maximum flux from the AZ to the microdomain around IP₃R cluster and K_c determines the half-maximal transfer rate.

$$J_{coupling} = V_c \frac{[Ca^{2+}_{AZ}]^2 - \bar{k}\big([Ca^{2+}_{IPR_n}]^2\big)}{[Ca^{2+}_{AZ}]^2 - K_c^2} \tag{6}$$

There is strong evidence that the expression of Ca²⁺ buffering proteins in AD-affected neurons is significantly lower than WT neurons [59—61]. We incorporate these observations in our model by using parameter values that results in a stronger coupling in AD-

affected bouton as compared to WT bouton. Although the choice of the model has its limitations, using a model that captures buffered Ca²⁺ diffusion becomes numerically intractable quickly as distances approach physiologically reasonable order of nanometers. Thus, this approach provides an extremely useful method to account for the interplay of $[Ca^{2+}_{AZ}]$ and $[Ca^{2+}_{IPR_n}]$.

2.2. IP₃R model

In the past, several models for IP₃Rs have been developed in WT and AD-affected cells [18, 62—64]. All these models are based on data obtained from non-neuronal cells. While these models can be used to make reliable qualitative predictions, our goal here is to quantify the effect of upregulated Ca²⁺ signaling on neurotransmitter release where a small difference in the open probability of the channel or dwell times can result in a significant change due to the small volume of the synaptic terminal. Thus, we developed a new four-state model to implement the kinetics of IP₃Rs (Fig. 2A). The channel has zero, two, two, and five Ca²⁺ bound when in the Resting (R), Active (A), Open (O), and Inactive (I) states, respectively. The transition rates between different states and the corresponding parameters are reported in Tables 5 and 6 respectively. As shown in Fig. 3, the model closely fits the kinetics of IP3R in neurons from WT and 3xTg AD mice observed in [21]. In the cluster, the gating of each IP₃R is regulated by the Ca²⁺ concentration in the microdomain around the cluster.

Table 4. IP₃ fluxes in the model.

Flux (reference)	Equation
PLCᵟ [57, 58]	$$J_{PLC} = \bar{V}_{PLC} \frac{\left(ca^{2+}_{cyt}\right)^2}{\left(ca^{2+}_{cyt}\right)^2 + K_{PLC}{}^2}$$ $$\bar{V}_{PLC} = V_{PLC} PLC$$ $$V_{PLC} = V_0 + V_Q \frac{q^2}{q^2 + K_Q{}^2}$$ $$q = H(t - t_1) * A\beta * e^{-r(t-t_1)H(t-t_1)}$$ $$\rho = V_R \frac{q}{q + K_R}$$ $$\frac{d}{dt} PLC = k_{f_{PLC}} G(PLC_{tot} - PLC) - k_{b_{PLC}} PLC$$ $$\frac{d}{dt} G = k_{f_G}(\rho + \delta)(G_{tot} - G) - k_{b_G} G$$
IP₃ Degradation [57]	$$J_{deg} = \left(\eta \frac{\left(ca^{2+}_{cyt}\right)^2}{\left(ca^{2+}_{cyt}\right)^2 + K_{IP3k}{}^2} + (1 - \eta) \right) IP_3$$ $$\eta = k_{3k}/\left(k_{3k} + k_{5p}\right)$$
Time constant of IP₃ turnover	$$\tau_{IP_3} = 1/\left(k_{3k} + k_{5p}\right)$$

228

229

Table 5. Transition rates used in the IP₃R model 230

Rate/parameter	Equation
Transition rates	$$k_{RA} = \left[1 \times \left(\frac{1}{j_{01}[Ca^{2+}]_{IPR_n}} + \frac{1}{j_{12}([Ca^{2+}]_{IPR_n})^2}\right)\right]^{-1}$$ $$k_{AR} = \left[K_A([Ca^{2+}]_{IPR_n})^2 \times \left(\frac{1}{j_{01}[Ca^{2+}]_{IPR_n}} + \frac{1}{j_{12}([Ca^{2+}]_{IPR_n})^2}\right)\right]^{-1}$$ $$k_{AO} = \left[K_A([Ca^{2+}]_{IPR_n})^2 \times \left(\frac{1}{j_{22}([Ca^{2+}]_{IPR_n})^2}\right)\right]^{-1}$$ $$k_{OA} = \left[K_O([Ca^{2+}]_{IPR_n})^2 \times \left(\frac{1}{j_{22}([Ca^{2+}]_{IPR_n})^2}\right)\right]^{-1}$$ $$k_{OI} = \left[K_O([Ca^{2+}]_{IPR_n})^2 \times \left(\frac{1}{j_{23}([Ca^{2+}]_{IPR_n})^3} + \frac{1}{j_{45}([Ca^{2+}]_{IPR_n})^5}\right)\right]^{-1}$$ $$k_{IO} = \left[K_I([Ca^{2+}]_{IPR_n})^5 \times \left(\frac{1}{j_{23}([Ca^{2+}]_{IPR_n})^3} + \frac{1}{j_{45}([Ca^{2+}]_{IPR_n})^5}\right)\right]^{-1}$$ $$k_{RI} = \left[1 \times \left(\frac{1}{\tilde{j}_{01}[Ca^{2+}]_{IPR_n}} + \frac{1}{\tilde{j}_{45}([Ca^{2+}]_{IPR_n})^5}\right)\right]^{-1}$$ $$k_{IR} = \left[K_I([Ca^{2+}]_{IPR_n})^5 \times \left(\frac{1}{\tilde{j}_{01}[Ca^{2+}]_{IPR_n}} + \frac{1}{\tilde{j}_{45}([Ca^{2+}]_{IPR_n})^5}\right)\right]^{-1}$$
Occupancy parameters	$$K_O = a_1 \frac{[IP_3]^{n_O}}{[IP_3]^{n_O} + K_{Od}{}^{n_O}}$$ $$K_A = a_2 \frac{[IP_3]^{n_A}}{[IP_3]^{n_A} + K_{Ad}{}^{n_A}}$$ $$K_I = a_2 \frac{[IP_3]^{n_I}}{[IP_3]^{n_I} + K_{Id}{}^{n_I}}$$

231

Table 6. Parameter values for the IP₃ dynamics and IP₃R. 232

Category/References	Parameters	Description	WT	AD
IP₃ Model (From [58])	V_0	PLC-mediated IP₃ production	0.15 μM	0.19 μM
	V_Q	Control parameter for influence of Aβ on IP₃	7.82 μM	380 μM
	K_Q	PLC dissociation constant	0.0086 μg/mL	0.0086 μg/mL
	K_{IP_3k}	Half-activation for 3-kinase	0.6 μM	1.6 μM
	K_{PLC}	PLC sensitivity to Ca²⁺	0.01 μM	0.016 μM
	k_{3k}	IP₃ phosphorylation rate	1.5 μs⁻¹	0.7 μs⁻¹
	k_{5p}	IP₃ dephosphorylation rate	0.01 μs⁻¹	0.005 μs⁻¹
PLC (Modified from [58])	$k_{f_{PLC}}$	PLC-protein activation rate	0.35 μs⁻¹	0.75 μs⁻¹
	$k_{b_{PLC}}$	PLC-protein deactivation rate	22 μs⁻¹	200 μs⁻¹
	PLC_{tot}	Scaled total number of PLC	1	1

G-Protein (From [58])	k_{f_G}	G-protein activation rate	0.33 μs^{-1}	0.047 μs^{-1}
	k_{b_G}	G-protein deactivation rate	2.17 μs^{-1}	4.7 μs^{-1}
	δ	G-protein intrinsic activity	0.01	0.012
	V_R	Maximal G-protein activation	7.4	10
	K_R	Aβ producing half-activation	4467 μg/mL	2000 μg/mL
	G_{tot}	Scaled total number of G-protein	1	1
IP₃R (Fit to Experiment)	a_1		17.05043 μM^{-2}	1.108278×10^2 μM^{-2}
	n_O		2.473407	2.473407
	K_{Od}		0.909078 μM	0.909078 μM
	a_2		18.49186 μM^{-2}	18.49186 μM^{-2}
	n_A		0.093452	0.093452
	K_{Ad}		1.955650 μM	1.955650 μM
	a_3		2.340259×10^2 μM^{-5}	1.4041556×10^2 μM^{-5}
	n_I		56.84823	56.84823
	K_{Id}		0.089938 μM	0.089938 μM
	j_{01}		3.031635×10^2 μM^{-1} ms^{-1}	3.031635×10^2 μM^{-1} ms^{-1}
	j_{12}		3.230063×10^2 μM^{-2} ms^{-1}	3.230063×10^2 μM^{-2} ms^{-1}
	j_{22}		4.814111 μM^{-2} ms^{-1}	5.3978052 μM^{-2} ms^{-1}
	j_{23}		5.356155 μM^{-3} ms^{-1}	2.0652269×10^3 μM^{-3} ms^{-1}
	j_{45}		5.625616 μM^{-5} ms^{-1}	5.4319289 μM^{-5} ms^{-1}
	$\tilde{j}_{01}$		3.013284×10^2 μM^{-1} ms^{-1}	3.013284×10^2 μM^{-1} ms^{-1}
	$\tilde{j}_{45}$		2.648741 μM^{-5} ms^{-1}	8.512829×10^{-8} μM^{-5} ms^{-1}

2.3. Membrane voltage dynamics

The basic equations for the membrane potential used in our model are adopted from Ref. [65]. Membrane potential (V) is governed by primary Na$^+$ (I_{Na}), K$^+$ (I_K), Cl$^-$ (I_{Cl}), and Ca^{2+} (I_{Ca}), currents, as well as current due applied stimulation (I_{app}), and is given as,

$$C_m \frac{dV}{dt} = I_{app} + I_{Na} + I_K + I_{Cl} + \left(\frac{I_{Ca}}{Area}\right)$$

where we assumed standard membrane capacitance C_m of $1 \frac{\mu F}{cm^2}$. The Na$^+$ and K$^+$ concentrations were assumed to be fixed, with corresponding currents consisting of active and passive leak components given by

$$I_{Na} = -(g_{Na} m_\infty{}^3 h)(V - E_{Na}) - g_{Na_{leak}}(V - E_{Na})$$

$$I_K = -\left(g_K n^4 + \frac{g_{AHP}[Ca^{2+}]_{cyt}}{1+[Ca^{2+}]_{cyt}}\right)(V - E_K) - g_{K_{leak}}(V - E_K)$$

Chloride currents only consist of passive leak contribution, defined by

$$I_{Cl} = -g_{Cl_{leak}}(V - E_{cl}).$$

The steady state gating activation and inactivation variables, as well as associated channel forward and reverse rates were calculated using the equations in Table 7. Various parameters used in the membrane potential equations are listed in Table 8.

2.4. Voltage gated Ca²⁺ channels

Consistent with findings in [66], we implement only the predominant high-threshold Cav2.1 (P/Q-type) channels present at presynaptic nerve terminals using a five-state kinetic scheme (see Fig. 2B). Voltage-dependent activation and deactivation rates for each closed state (I = 1, 2, 3, 4) were respectively calculated as follows: $\alpha_i(V) = \alpha_{i0} \exp(V/k_i)$, $\beta_i(V) = \beta_{i0} \exp(V/k_i)$, where values for activation and deactivation rates at 0 mV, α_{i0} and β_{i0}, and for slope factor k_i were taken from [66] and listed in Table 8. As with the IP₃Rs, we model VGCC gating stochastically as a discrete-time Markov Chain (DTMC) (*see section 2.7 Numerical Methods*). Single channel Ca²⁺ currents were calculated using $I_s = gP_o(V - E_{Ca^{2+}})$, where values for conductance g, extracellular Ca²⁺ concentration and Nernst potential $E_{Ca^{2+}}$ were obtained from [53] and are reported in Table 8.

Table 7. Parameter values for membrane potential equations.

| Parameter	Value / Units [65]	Description
C_m	1 µF/cm²	Membrane Capacitance
g_{Na}	120 mS/cm²	Maximum Conductance for active Na⁺ channels
$g_{Na_{leak}}$	0.0175 mS/cm²	Conductance for Na⁺ passive leak channels
g_K	36 mS/cm²	Maximum Conductance for active K⁺ channels
$g_{K_{leak}}$	0.05 mS/cm²	Conductance for K⁺ passive leak channels
$g_{Cl_{leak}}$	0.05 mS/cm²	Conductance for Cl⁻ passive leak channels
ϕ	5.0	
g_{AHP}	0.01	
α_n	$\dfrac{0.01(V + 34)}{1 - \exp\left(-\dfrac{V + 34}{10}\right)}$	Forward rate for K⁺ current activation gating variable
β_n	$0.125 \exp\left(-\dfrac{V + 44}{80}\right)$	Backward rate for K⁺ current activation gating variable
α_h	$0.07 \exp\left(-\dfrac{V + 44}{20}\right)$	Forward rate for Na⁺ current inactivation gating variable
β_h	$\dfrac{1}{1 + \exp\left(-\dfrac{V + 14}{10}\right)}$	Backward rate for Na⁺ current inactivation gating variable
α_m	$\dfrac{0.1(V + 30)}{1 - \exp\left(-\dfrac{V + 30}{10}\right)}$	Forward rate for Na⁺ current activation gating variable
β_m	$4 \exp\left(-\dfrac{V + 55}{18}\right)$	Backward rate for Na⁺ current activation gating variable

m_∞	$\dfrac{\alpha_m}{\alpha_m + \beta_m}$	Occupancy of Na+ activation gating variable
	$\dfrac{dn}{dt} = \phi(\alpha_n(1-n) - \beta_n n)$	Evolution occupancy of gating K+ current gating variable
	$\dfrac{dh}{dt} = \phi(\alpha_h(1-h) - \beta_h h)$	Evolution occupancy of gating Na+ current inactivation gating variable

271

Table 8. Reaction rates for kinetic schemes for VGCC.   272

Parameter	Value / Units	Notes
$\alpha_{10}, \alpha_{20}, \alpha_{30}, \alpha_{40}$	4.04, 6.70, 4.39, 17.33 ms^{-1}	From [66, 67]
$\beta_{10}, \beta_{20}, \beta_{30}, \beta_{40}$	2.88, 6.30, 8.16, 1.84 ms^{-1}	From [66, 67]
k_1, k_2, k_3, k_4	49.14, 42.08, 55.31, 26.55 mV	From [66, 67]

273

2.5. Overall release model   274

The complete release scheme has been adopted and modified from [68] (see Fig. 2C   275
& 2D). In addition to the Ca2+—dependent vesicle mobilization and priming steps, we re-   276
place the independence of Ca2+ binding to C2A and C2B domains of synaptotagmin with   277
the dual sensor model proposed in [69], where two independent Ca2+ sensors act in paral-   278
lel to trigger distinct pathways of exocytosis that lead to fast synchronous, slow asynchro-   279
nous, and spontaneous release. Synchronous release is mediated by the sensor S with 5   280
Ca2+-binding sites and cooperativity (b) incorporated to progressively decrease backward   281
rates— Ca2+ unbinding. Synchronous fusion occurs when all 5 binding sites are occupied.   282
Likewise, the sensor A—with 2 Ca2+-binding sites—mediates asynchronous release with   283
the same cooperativity parameter b. Spontaneous release is also included and occurs at a   284
much slower rate when the sensors have no Ca2+ bound. As in [67], release rates and model   285
parameters were obtained according to fits to experimental data reported in [70]. Contrary   286
to the dual sensor model of [71], we do not assume the synchronous (γ_2) and asynchro-   287
nous (γ_3) release rates to be the same. This is because according to [67], hippocampal re-   288
lease rates from [70] could not be fitted otherwise. Consequently, we use the release rate   289
for the asynchronous release to be $a\gamma$ where *a* = 0.025.   290

291
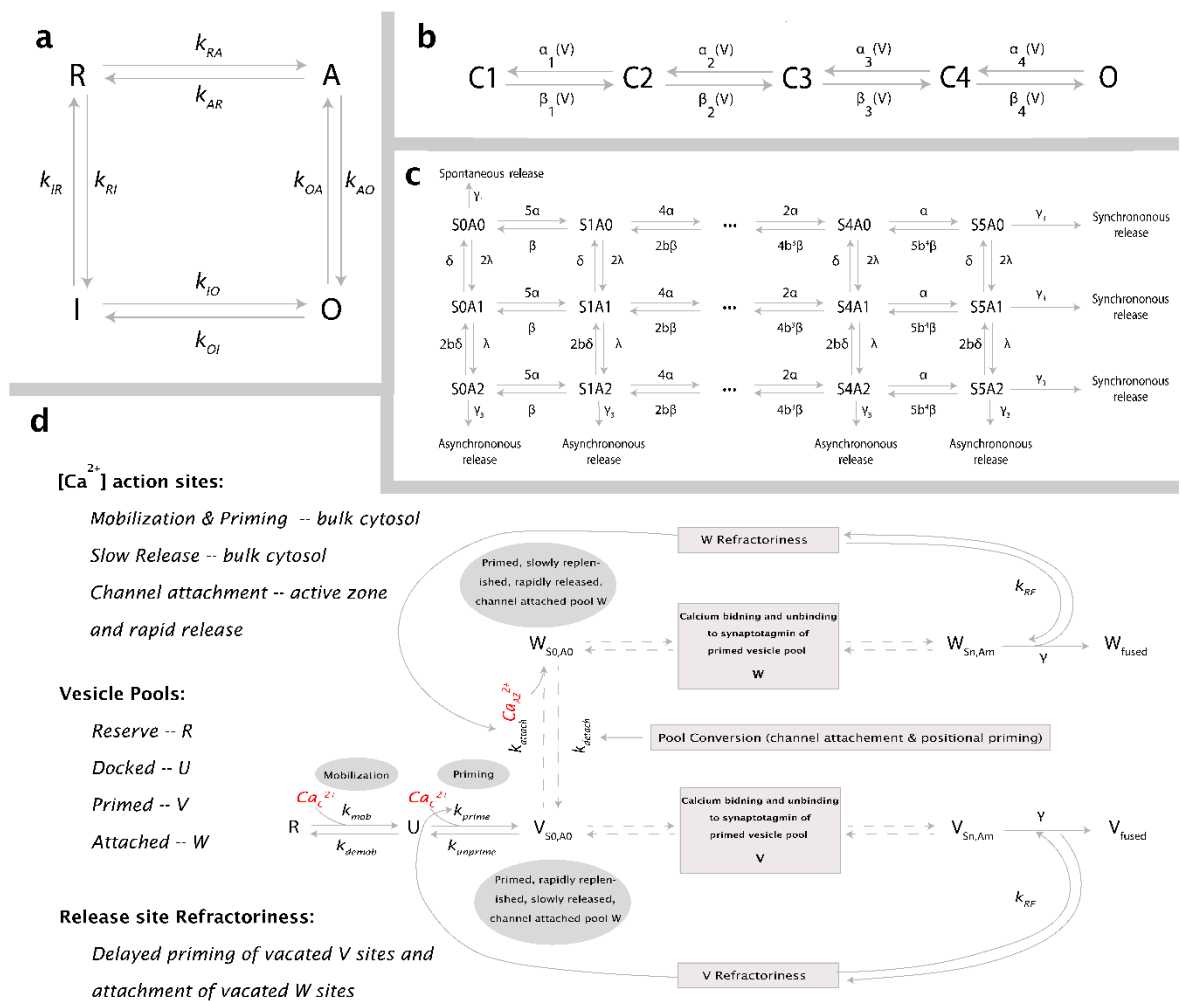
Figure 2. Kinetic schemes used in the model: (**A**) Gating kinetics of IP₃R. Four-state model representing the possible states along with corresponding transition rates; (**B**) Model for VGCC gating with four closed states (C1 - C4) and one open Ca²⁺ conducting state (O); (**C**) Scheme for Ca²⁺ binding to Synaptotagmin with dual Ca²⁺ sensors for fast synchronous (S with five Ca²⁺-binding sites), slow asynchronous (A with two Ca²⁺-binding sites), and spontaneous exocytosis; (**D**) Modified from [27], the overall release scheme which includes vesicle mobilization from a reserve pool (R) to docked, unprimed pool (U), molecular priming to vesicles unattached to a Ca²⁺ channel (V), and conversion to vesicles coupled to a VGCCs cluster (W). Both vesicle pools are released through the dual sensor release model. Channel attached vesicles are steeply dependent on $[Ca_{AZ}^{2+}]$, whereas $[Ca_{cyt}^{2+}]$ governs the release of detached vesicles. Reaction rates along with respective references are listed in Tables 6, 8, and 9.

As described in [69] and shown in Fig. 4, compared to the Allosteric model, this model captures the expected heterogeneity and latency of exocytosis more accurately at the Calyx of Held. Apart from the intrinsic heterogeneity of release pathways, the model implemented here captures the heterogeneity of vesicle pools—slow and fast—, where docking and priming are part of the upstream processes for recruiting vesicles into the Slow-Releasing Pool (SRP) and super-priming of vesicles in the SRP aids the conversion of SRP vesicles to those in the Fast-Releasing Pool (FRP). The recruitment of vesicles into the SRP is dependent on the cytosolic $[Ca_{cyt}^{2+}]$, whereas channel attachment is aided by Ca²⁺ influx. As described in Fig 2, the target of Ca²⁺ mediating vesicle fusion depends on which pool the fusing vesicle belongs to; for vesicles in the FRP, this is $[Ca_{AZ}^{2+}]$, while those in the SRP bind $[Ca_{cyt}^{2+}]$.

We also include release site refractoriness introduced in [67, 68] in order to simulate 314
experimental observations. In this context, a vesicle cannot be released from a vacated site 315
for a period determined by k_{RF}, such that sites—either Ca²⁺-attached (*W*) or detached 316
(*V*)—from which vesicles had been released remain unable to accept a new primed vesicle 317
for some time. Phasic synapses are known to have briefer refractoriness compared to their 318
tonic counterparts, and as such, we choose k_{RF} to be 0.01 ms⁻¹, similar to values observed 319
at hippocampal synapses in [72]. Different parameters used in the release model are listed 320
in Table 9. 321

322

Table 9. Reaction rates for kinetic schemes for exocytosis. 323

Parameter	Value / Units	Description	Notes
k_{mob}	Mobilization rate	5.0×10^{-5} μM⁻¹ms⁻¹	From [68]
k_{demob}	Demobilization rate	0.0022 ms⁻¹	From [68]
$k_{priming}$	Priming rate	0.027990 μM⁻¹ms⁻¹	From [68]
k_{unpr}	Unpriming rate	0.005356 ms⁻¹	From [68]
k_{attach}	Attachment rate	0.0015 μM⁻¹ms⁻¹	Fit
k_{detach}	Detachment rate	0.001158 ms⁻¹	Fit
k_{RF}	Refractoriness	10.34-1 ms⁻¹	Fit
α	Association rate for synchronous release	0.061200 μM⁻¹ms⁻¹	From [67]
β	Dissociation rate, synchronous release	2.32 ms⁻¹	From [67]
λ	Association rate for Asynchronous release	0.002933 μM⁻¹ms⁻¹	Fit
δ	Dissociation rate for Asynchronous release	0.014829 ms⁻¹	Fit
γ_1	Spontaneous release rate	9×10^{-6} ms⁻¹	Fit
γ_2	Synchronous release rate	2.000008 ms⁻¹	From [67]
γ_3	Asynchronous release rate	$a \cdot \gamma_2$ ms⁻¹	From [67]
b	Cooperativity factor	0.250007	From [67]
a		0.025007	From [67]

324

2.6. Synchrony measure 325

For a wide range of synaptic configurations with distinct intrinsic release probabili- 326
ties, we computed the synchrony of AP arrival times (estimated at peak) and release event 327
times using a modified version of the Pinsky-Rinzel measure of synchrony [73]. We 328
transformed the firing times $T(k)$ for every *k^th* event of the neuron into a set of corre- 329
sponding vector phases $\phi(k)$ using Eq. 7, where $T_{AP}(k)$ corresponds to all the AP events 330
within the duration of simulation. For each vector phase $\phi(k)$, we compute the synchrony 331

$r(\phi(k))$—numbers between 0 and 1—using the complex order parameter defined by Strogatz and Mirollo averaged across all events for a single synaptic configuration [74] (Eq. 8).

$$\phi(k) = \frac{T_{AP}(k) - T(k)}{T(k+1) - T(k)} \qquad (7)$$

$$r(\phi(k)) = \frac{1}{N_K} \sum e^{(2\pi i \phi(k))} \qquad (8)$$

2.7. Numerical Methods

Deterministic equations (Eqs. 1-4) are solved using the fourth-order Runge-Kutta algorithm (RK4) with a 1 μs time step, while the stochastic states of the IP3Rs and VGCCs determined by the corresponding kinetic schemes were simulated using a procedure outlined in [75], which is equivalent to the Gillespie algorithm with fixed time step. All numerical simulations were performed in MATLAB (The MathWorks, Natick, MA) and data analysis was carried out using custom Python scripts (version 3.9).

3. Results

3.1. The gain-of-function enhancement of IP3R gating in FAD

The exaggerated Ca2+ release observed in FAD-affected neurons is ascribed mainly to the gain-of-function enhancement of IP3Rs in the affected cells due to FAD-causing mutations in presenilin [18, 19, 21, 76, 77]. Indeed, it has been shown that cell models expressing PS mutations exhibit a several-fold increase in the open probability (Po) of IP3Rs [19, 76]. Specifically, the Po of IP3R in cortical neurons from 3xTg-AD mice carrying PS mutations was enhanced by 700% relative to control mice with wildtype (WT) PS (0.43 ± 0.05 in AD versus 0.06 ± 0.01 in WT mice) at $[Ca_{cyt}^{2+}]$ of 1 μM and IP3 concentration ($[IP_3]$) of 10 μM [21]. Given that all models for IP3R in WT or AD-affected cells are based on non-neuronal cells, we use the above findings to build a new model for the gating kinetics of IP3Rs in neurons from WT and 3xTg-AD mice (see details in *Materials and Methods*). Parameters yielding the best fit to experimental observations are listed in Table 6.

Our model mimics the gating of IP3R in neurons from WT and 3xTg-AD mice (Fig 3), closely reproducing the observed values of the *Po* (Fig 3A, D), mean open time (τ_o) (Fig 3B, E), and mean close time (τ_c) (Fig 3C, F) reported in [21]. The significantly higher *Po* of the channel in FAD-affected neurons is reflected in the time-traces from the model, showing that the channel spends significantly more time in the open state in the diseased state (Fig 3G). To determine how the observations about different resting $[Ca_{cyt}^{2+}]$ in AD-affected cells change the behavior of IP3Rs, we plot the *Po* of the channel as a function of [Ca2+]c and $[IP_3]$ (Fig. 3H, I). Previous studies of 3xTg and APPSW AD mice models reported resting $[Ca_{cyt}^{2+}]$ of *247 $\pm$ 10.1 nM* and *225.2 $\pm$ 11.7 nM* respectively, whereas $[Ca_{cyt}^{2+}]$ of *110.8 $\pm$ 1.5 nM* was recorded in WT mice [78]. In particular, cortical neurites of plaque bearing mice express a 6-fold increase in resting $[Ca_{cyt}^{2+}]$ relative to non-transgenic mice [11]. Here, our model exhibits a 4.42-fold increase in *Po* of IP3Rs in WT neurons as we increase $[Ca_{cyt}^{2+}]$ from 110 nM to 250 nM (0.005626 vs 0.02484) at 0.3 μM $[IP_3]$. At $[IP_3]$ = 0.3 μM and $[Ca_{cyt}^{2+}]$ = 250 nM, *Po* of the channel in FAD-affected neurons reaches 0.2565—a 10.32-fold increase relative to WT neurons (Fig 3H, I). Thus, our model predicts that an IP3R in FAD-affected neurons will exhibit an almost 45-fold increase in *Po* compared to control neurons with the same amount of IP3, leading to a significantly higher Ca2+ release from the ER.
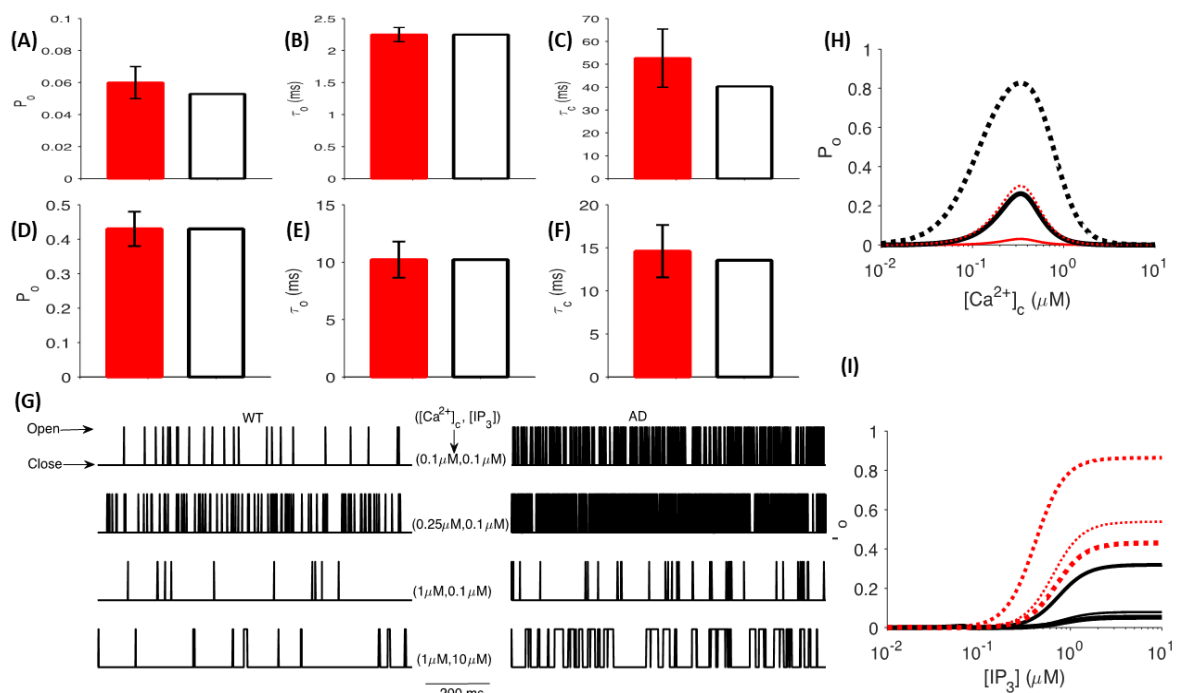
Figure 3. Gain-of-function enhancement of IP₃R gating in FAD: The P_o (**A, D**), τ_o (**B, E**), and τ_c (**C, F**) of IP₃R given by the model (empty bars) and observed values in primary cortical neurons from WT (**A-C**) and 3xTg AD mice (filled bars) (**D-F**) at $[Ca_{cyt}^{2+}]$ = 1 μM and $[IP_3]$ = 10 μM; (**G**) Sample time-traces generated by stochastically simulating a single IP₃R channel in cortical neurons from WT (left column) and AD (right column) mice at different $[Ca_{cyt}^{2+}]$ and $[IP_3]$ values shown in the figure; (**H**) P_o of IP₃R as a function of $[Ca_{cyt}^{2+}]$ at $[IP_3]$ = 0.3 μM (thin lines) and 1 μM (thick lines) in WT (solid lines) and AD-affected (dotted) neurons; (**I**) P_o of IP₃R as a function of $[IP_3]$ at $[Ca_{cyt}^{2+}]$ = 0.1, 0.25, and 1 μM (the increasing value of $[Ca_{cyt}^{2+}]$ is represented by the thickness of the line) in WT (solid lines) and AD-affected (dotted) neurons. Experimental values shown for comparison in (**A-F**) are from [21].

3.2. Characterization of the glutamate release model and release event

We next examine the relationship between total release from a single process following $[Ca_{cyt}^{2+}]$ clamps at different concentration steps. We observe that the release rate rapidly increases and transiently decays back to basal level within tens of milliseconds—a result of the sensitivity of the Ca²⁺ sensors (Fig 4A). For comparison, we also show the release rate given by the Allosteric model at different $[Ca_{cyt}^{2+}]$ values (Fig. 4B). Also, we obtain results similar to quantitative studies of transmission profiles in Calyx-of-Held synapse, where release profiles were quantified from deconvolution of evoked miniature excitatory postsynaptic current waveforms [69]. Unsurprisingly, we observed a shift in the $[Ca_{cyt}^{2+}]$ dependency of the peak release rate as the response to clamped intracellular Ca²⁺ levels is both lower and right-shifted relative to the experimental data for the Calyx-of-Held (Fig 4C), whereas the time delay (time-to-peak) of peak release rate shows higher and right-shifted exponential decay (Fig 4D). This is consistent with observations of approximately hundred-fold decrease in total vesicle population in hippocampal boutons [51, 79]. In addition, our model mimics the Ca²⁺-dependent increase in release rate observed at high fidelity synapses of cerebellar mossy fiber boutons (cMFBs), which permit direct presynaptic recordings and are reported to have high structural similarities with their hippocampal counterparts (Fig 4C) [80, 81]. Moreover, in agreement with previous recordings of spontaneous release events from CA3-CA1 synapses, we affirmed that the spontaneous release rate elicited by resting level $[Ca_{cyt}^{2+}]$ of 100 nM is within the reported range of 10⁻⁴ and 10⁻⁵ per ms [53, 82, 83]. The Dual-Sensor model is more in line with the findings on CA3-CA1 synapses and is used throughout this work. However, it should be mentioned
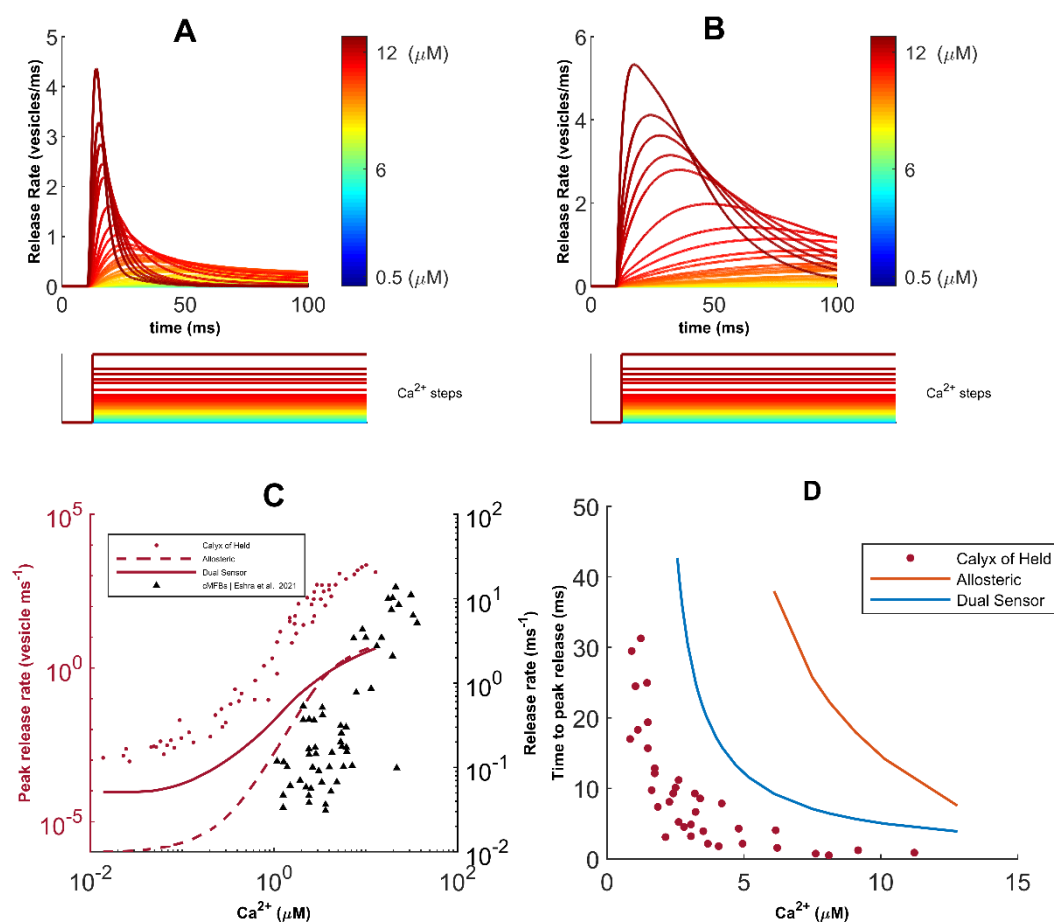
Figure 4. Characterization of neurotransmission in response to $[Ca_{cyt}^{2+}]$ steps: (**A**) Total release events
obtained from a single Dual-Sensor fusion process after clamping $[Ca_{cyt}^{2+}]$ at different values; (**B**)
Release profile following Allosteric fusion in response to stepwise $[Ca_{cyt}^{2+}]$ clamp; (**C**) Regulation of
the peak release rate in response to clamped $[Ca_{cyt}^{2+}]$ levels show lower and right-shifted dose-re-
sponses relative to the experimental data for the Calyx-of-Held; (**D**) $[Ca_{cyt}^{2+}]$ dependence of time-to-
peak rate indicates exponentially decreasing but longer time delay to peak release when matched
with data for the Calyx-of-Held. Experimental values shown for comparison in (**C, D**) are from [80].

that some technical details may prevent direct comparison to exocytosis at cMFBs where
the release rate is obtained as the inverse of exponential fits to the cumulative release ob-
tained from deconvolution analysis and reflects the release rate constant per vesicle.
Therefore, the comparison between our model and these findings must be viewed cau-
tiously [69, 80].

3.3. FAD-associated intracellular Ca²⁺ changes enhance neurotransmitter release

Several studies have reported enhanced Ca²⁺ release from the ER in AD-affected neu-
rons [84—88]. This enhanced Ca²⁺ release has been associated with the several fold in-
crease in the P_o of IP₃Rs observed in multiple animal and human cell models of FAD [18,
19, 21, 78, 85]. Although presynaptic plasticity and synaptic vesicle release (SVR) are
tightly coupled to Ca²⁺ entry through VGCCs, several studies have established an im-
portant role for ER stores in regulating presynaptic plasticity and neurotransmission [28,
34, 35, 89, 90]. Furthermore, strong experimental evidence supports the existence of a feed-
back loop between the ER Ca²⁺ stores and AP triggered exocytosis events [91]. Accord-
ingly, here we explore how the observed gain-of-function enhancement of IP₃Rs in FAD
affects neurotransmitter release. In addition to enhanced Ca²⁺ release through IP₃Rs,

432
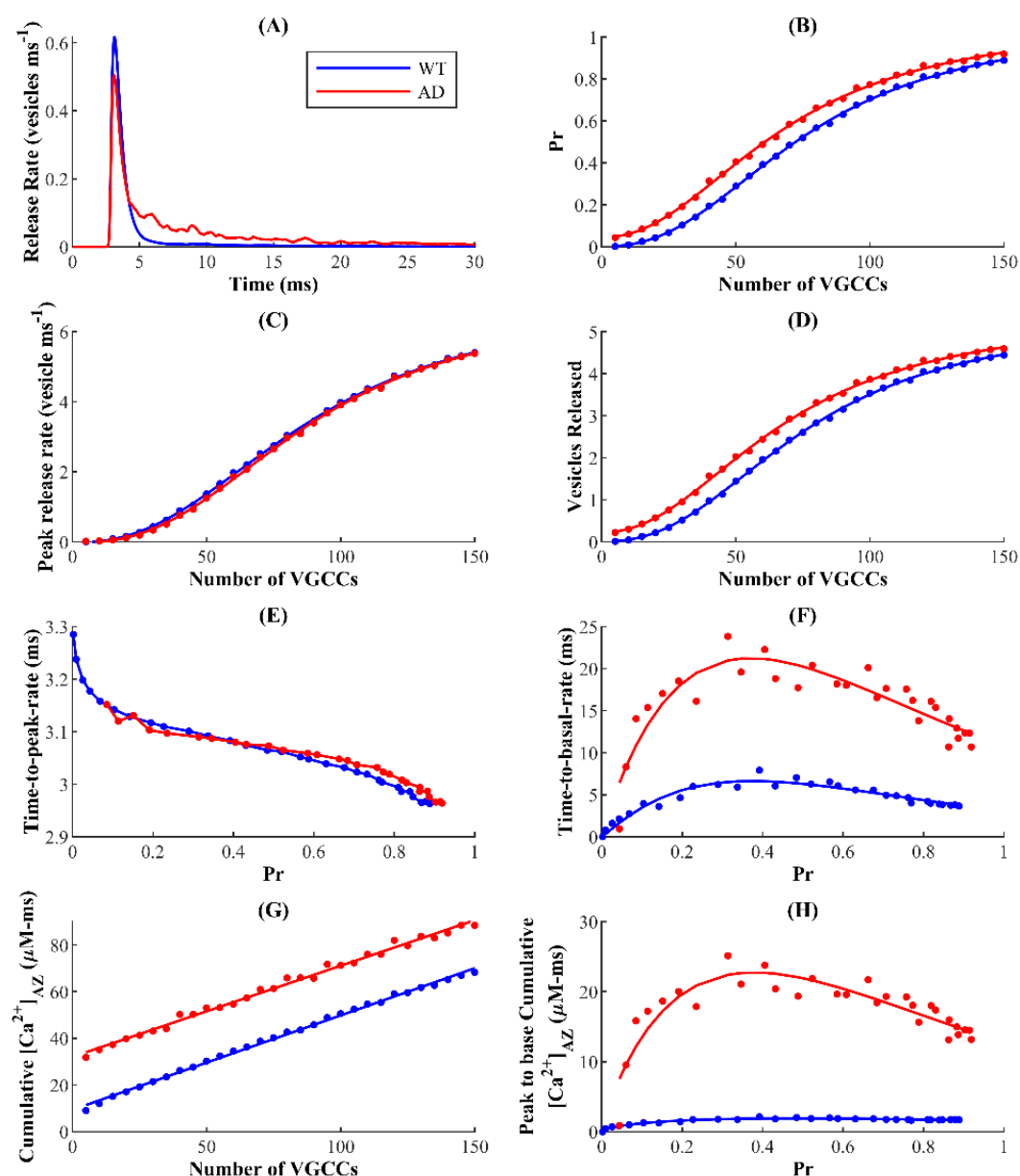
Figure 5. ER-driven upregulation of cytosolic Ca²⁺ leads to enhanced synaptic vesicle release in FAD: (**A**) Neurotransmitter release rate in response to a single AP in WT and AD-affected synapse. Change in the P_r of a single synaptic vesicle (**B**); peak release rate (**C**); and the average number of vesicles released (**D**) as functions of the number of VGCCs; (**E**) Time delay of peak release rate; and (**F**) decay time to basal release rate as functions of P_r; (**G**) Change in $[Ca^{2+}_{AZ}]$ with number of VGCCs; (**H**) Cumulative Ca²⁺ from peak to basal level as a function of P_r.

multiple studies have implicated a significant downregulation of Ca²⁺ buffering proteins in FAD-affected neurons as compared to WT neurons [59—61]. We incorporate the effect of observed changes in Ca²⁺ buffering proteins by considering two configurations: High

Coupling (HC) and Normal Coupling (NC) between the ER and AZ. The HC configuration corresponds to the downregulation of Ca^{2+} buffering proteins (see more details in *Materials and Methods*) (Supplementary Fig 1).

In Fig. 5A, we show a typical release profile in response to a single AP, where a clear difference between WT and FAD-affected synapses can be seen. To quantify this difference, we compute the release probability (P_r) by counting the number of vesicles released from the slow and fast release-ready pools (RRP), divided by the number of vesicles initially in both pools. In FAD-affected synapse, we observe enhanced P_r over a wide range of VGCC expressions in dose-response manner (Fig 5B), suggesting that the acute effects of FAD-driven aberrant cytosolic Ca^{2+} are not exclusive to synapses operating in the regime of sparse VGCCs. Surprisingly, we observe only a marginal difference in the peak release rate between WT and FAD-affected synapses (Fig 5C). We also calculated the number of vesicles released during a single AP by integrating the rate of vesicle release from the slow and fast RRP and noticed a significant increase in vesicles released in the FAD-affected synapse (Fig. 5D). To discern the contribution of enhanced Ca^{2+} release through IP$_3$Rs from that due to the HC, we simulate four scenarios: (1) enhanced Ca^{2+} release through IP$_3$Rs but NC (AD-NC), (2) enhanced Ca^{2+} release through IP$_3$Rs with HC (AD-HC), (3) normal Ca^{2+} release through IP$_3$Rs and NC (WT-NC), and (4) normal Ca^{2+} release through IP$_3$Rs and HC (WT-HC). We notice that while HC causes a minor increase in the release probability and vesicles released in the WT synapse, it strongly affects both these features in the FAD-affected synapse (Supplementary Fig 2A, B).

To gain deeper insight into the observed changes in the P_r, we examine the dependence of the release rise time (Time to peak release rate) on P_r (P_r is increased by increasing the number of VGCCs as in Fig 5A) and observed no significant differences between FAD-affected and WT synapses (Fig 5E). Interestingly, the decay time (Time to basal release rate) exhibits a biphasic dependence on P_r with a longer decay time in FAD-affected synapses. Strikingly, the decay time as well as the concomitant FAD-associated enhancement is attenuated in synapses with both high and low P_r, and peaks at P_r corresponding to physiologically reasonable VGCCs expression for small hippocampal synapses [84], suggesting that such small hippocampal synapses are more sensitive to alternations due to FAD-associated Ca^{2+} disruptions (Fig 5F). Like the release probability as a function of time and vesicles released during a single AP, HC has a stronger effect on the release rise time mainly due to the changes in Ca^{2+} in AZ in the FAD-affected synapse (Supplementary Fig 2C, D).

To assess the direct correspondence between the changes in different aspects of SVR and enhanced Ca^{2+} release, we examine the cumulative Ca^{2+} at AZ. The elevated Ca^{2+} release from the ER maintains larger cumulative Ca^{2+} (area under the Ca^{2+} transient) at AZ in the FAD-affected synapse consistently across a wide range of VGCCs expression, in agreement with several studies showing that ER Ca^{2+} channels can sculpt the spatiotemporal dynamics of exocytosis and consequently neuronal function (Fig 5G) [92, 93]. However, this continuous enhancement as a function of VGCCs expression is not consistent with the biphasic behavior of the time to basal rate as a function of P_r. Next, we examined the residual Ca^{2+} in the AZ, obtained as the cumulative Ca^{2+} that persists during decay phase of the Ca^{2+} transient. Our results show that larger residual Ca^{2+} in FAD-affected synapses also exhibits a biphasic behavior as a function of P_r similar to the time to basal neurotransmitter release rate. Again, this enhancement was non-uniform, suggesting that small hippocampal synapses with intermediate P_r values are highly sensitive to pathological alterations (Fig 5H). Taken together, our data reveal that ER-driven Ca^{2+} disruption plays a critical role in shaping the observed response profile, with the acute effects induced by such disruptions more severely expressed in small hippocampal synapses. Our results also show that these effects are more sensitive to the coupling between the Ca^{2+} domains in the vicinity of VGCCs and ER in FAD-affected synapses (Supplementary Fig 2C, D), consistent with reports on the involvement of ER Ca^{2+} in the regulation of presynaptic resting $[Ca^{2+}]_c$ and neurotransmission [91—93]. Furthermore, the sensitivity to the

coupling between the Ca²⁺ domains is exacerbated for synapses with intermediate P_r values (Supplementary Fig 2C, D).

3.3. Very short-term plasticity is enhanced in the FAD-affected synapse

Next, we investigate how the enhanced Ca²⁺ release from the ER affects very short-term presynaptic plasticity (STP). STP is assessed by determining the paired-pulse ratio (PPR): a classical measure of presynaptic modulation in response to paired stimuli separated by very short time interval [72]. After stimulating the nerve terminal with two pulses separated by a 40 ms interval (Fig 6A), we define PPR as the ratio of the P_r following the second pulse (Pr_2) to that of the first pulse (Pr_1) averaged over several trials. Therefore, the response to the second stimulus can either be enhanced with $Pr_2/Pr > 1$ (short-term facilitation (STF)) or depressed with $Pr_2/Pr < 1$ (short-term depression (STD)).
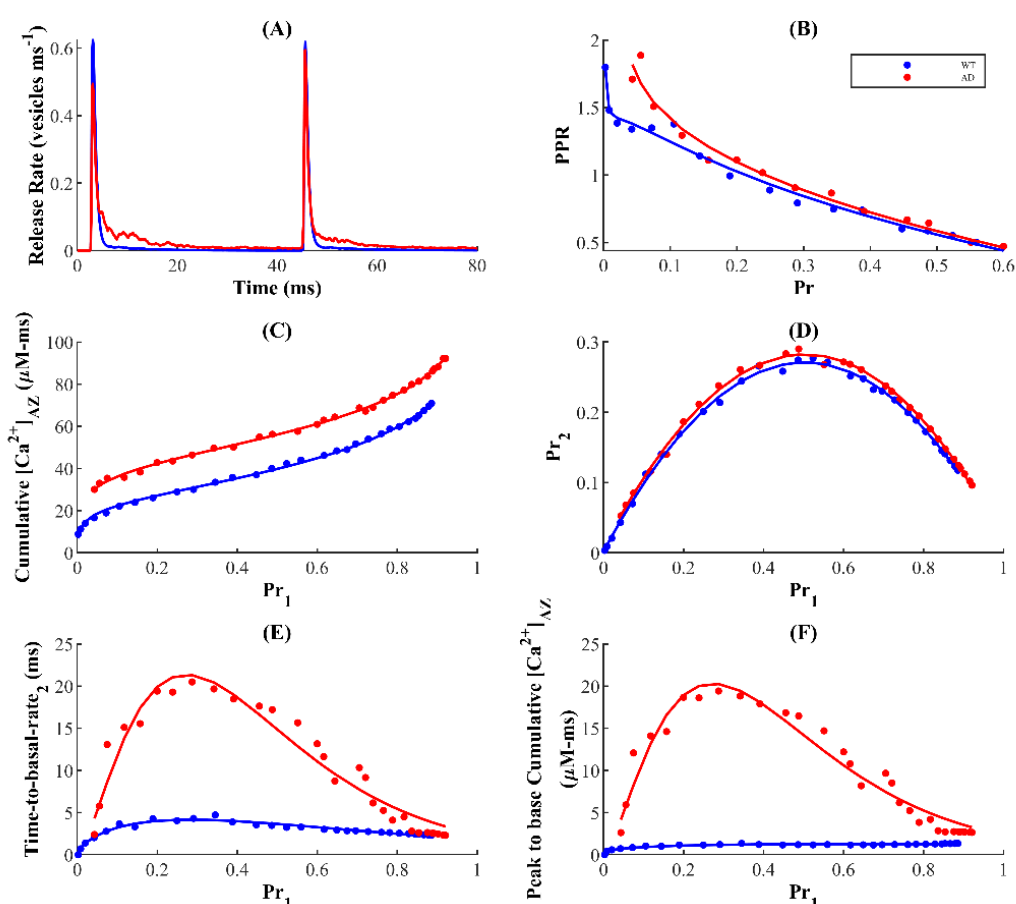
Figure 6. FAD-associated Ca²⁺ upregulation enhances STF: (**A**) Release profile following paired-pulse stimulation protocol; (**B**) PPR is inversely related to intrinsic P_r (obtained after first pulse), and is higher in the AD-affected synapse; (**C**) Similar to the first pulse *(Fig 3G)*, cumulative $[Ca_{AZ}^{2+}]$ after the second pulse increases with the P_r and is higher in AD-affected synapse; (**D**) Pr in response to the second pulse (Pr_2 as a function of P_r following the first pulse (Pr_1 Higher values indicate that the synapse responds more strongly to the subsequent stimulus in a paired-pulse protocol; (**E**) Decay time of release rate after second pulse also exhibits a biphasic behavior; (**F**) Cumulative $[Ca_{AZ}^{2+}]$ following the second pulse reflects the biphasic behavior observed in time delay of peak-to-basal release rate in panel **E**.

On average, both WT and FAD-affected synapses exhibited an inverse relationship between Pr_1 and the PPR, consistent with previous findings in phasic synapses such as small glutamatergic synapses in the hippocampus (Fig 6B) [93, 94, 95]. This negative correlation, thought to be a universal feature of these synapses, is assumed to be caused by the spike-driven depletion of vesicles in the RRP after the first pulse which is unlikely to be recovered by Ca²⁺-driven facilitation upon the next stimulation. Therefore, whether a synapse exhibits STF or STD is largely dependent on the recent activation history, which implies that synapses with large number of VGCCs and consequently very high intrinsic release probabilities tend to depress their response more severely to a second pulse, allowing them to operate at low PPR [25, 72, 93—96].

While additional mechanisms may contribute to STD, the depletion model of depression in phasic synapses suggests that at rest, the priming sites containing the RRP of vesicles is mostly occupied and reflects the inability of residual Ca²⁺—left over from the previous stimulation—and the incoming flux to potentiate release during the second stimulation [24, 68]. In agreement with these findings, our model establishes the dynamic equilibrium between the RRP (primed pool) and the unprimed pool by ensuring a relatively faster priming rate. As a result, we find here that most synapses operating in the intermediate-release-probability regime, characteristic of hippocampal excitatory synapses, display low STD with PPR < 1 in both WT and disease states (Fig 6B). Strikingly, FAD-affected synapse displays enhanced presynaptic strength relative to WT synapse, in contrast to the notion that the activity-dependent tunability of PPR ensures that periods of elevated activity results in subsequently depressed response. A simple explanation for this is that in the FAD-affected synapse, the elevated residual Ca²⁺ in the nerve terminal after the conditioning stimulus is longer-lasting and facilitates additional release upon subsequent stimulation (Fig 6A). To test the veracity of this claim, we examined whether the $[Ca_{AZ}^{2+}]$ remains elevated following the second pulse. Consequently, we find that the FAD-associated enhancement of residual $[Ca_{AZ}^{2+}]$ is sustained after the second stimulation and increases with Pr_1 (Fig 6C). These results suggest that on short timescales, the reduced depression observed in FAD-affected synapses is orchestrated by Ca²⁺ released from internal stores and induces a history-dependent enhancement of STP with respect to the WT synapse.

Although our results suggest that higher-probability synapses consistently express greater depression, it is still unclear whether probability of transmission of consecutive spikes monotonically relates to intrinsic release probability, and what role the ER plays in sculpting the concomitant profile. For this purpose, we examine the Pr_2 as a function of Pr_1 (Fig 6D), which reflects the conditional probability that a successful release event on the first pulse is followed by another successful release on the second pulse. Our data reveal that the success of a transmission event in response to the second stimulus depends on that for the first stimulus in a bell-shaped manner, indicating that the probability of vesicle release upon consecutive spikes is attenuated at both low and high probability synapses. This implies that synapses with intermediate number of VGCCs display higher success of transmission of consecutive spikes, in agreement with the idea that the stochasticity/unreliability of transmission probability can enhance the efficacy of information transmission across the synapse [97—99]. Unsurprisingly, the FAD-affected synapse facilitates transmission in response to the second stimulus more strongly compared to the WT synapse. This suggests that diseased synapses retain longer history of Ca²⁺ events, which consequently contributes to hyperactivation of release at short time scales. To verify this claim, we examined whether the biphasic response of the decay time and cumulative $[Ca_{AZ}^{2+}]$ due to the first stimulus is sustained after the second stimulus. Indeed, we observe that both decay time and cumulative $[Ca_{AZ}^{2+}]$ retain their bell-shaped dependence on Pr_1 (Fig 6E & 6F). Importantly, the FAD-affected synapse exhibits markedly enhanced response to the second stimulus following the elevated residual $[Ca_{AZ}^{2+}]$ due to the first pulse, in agreement with the notion that FAD-affected synapses can result in enhanced

excitation of neuronal processes. These findings are consistent with previous work show-
ing that, particularly in the early stages of FAD, over-excitation dominates neuronal cir-
cuits with soluble Aβ oligomers and contributes to cognitive dysfunction and impair-
ments [84, 101, 102]. In summary, FAD-associated enhanced Ca^{2+} release from intracellular
stores leads to a history-dependent enhanced STP and hyperactivation of neuronal pro-
cesses at short time scales with respect to WT synapses. We also notice that the higher
coupling strength between the AZ and microdomain of IP3Rs cluster exacerbate the en-
hanced PPR but has a marginal effect on the bell-shaped behavior of Pr_2 as a function of
Pr_1 in FAD-affected synapses (Supplementary Fig 3).

*3.4. FAD-associated Ca^{2+} rises differentially regulate synchronous and asynchronous release
during repetitive stimulation*

Next, we investigate the effect of upregulated cytosolic Ca^{2+} on synaptic response fol-
lowing trains of stimuli. As in the previous section, we stimulate the synapse with a train
of 20 APs delivered at 20 Hz and defined facilitation as the ratio of response following the
n^{th} stimulus (R_n) to that of the first (R_1) averaged over several trials. Therefore, synaptic
response to successive stimuli in the pulse train can either be depressed, with $R_n/R_1 < 1$,
or facilitated, with $R_n/R_1 > 1$. In both WT and FAD-affected synapses, repetitive activa-
tion leads to depression of both peak release rate (Fig 7a) and P_r (Fig 7b) that increase with
subsequent stimuli. Here, the FAD-affected synapses exhibits lower peak release rate (Fig.
7C) and baseline P_r (Fig. 7D) leading to lower facilitation that persists throughout activa-
tion. The depression due to higher-frequency longer (~450 msec) stimulus train observed
in the FAD-affected synapse results from rapid depletion of the vesicles in the RRP rela-
tive to the WT synapse (Fig 7E).

Although evoked peak release rate and P_r exhibit similar decay as functions of pulse
number, FAD-associated Ca^{2+} disruptions differentially affect these two properties. While
the peak release rate in case of the WT synapse remains mostly higher than that of the
FAD-affected synapse, the P_r in case of FAD-affected synapses is consistently higher fol-
lowing successive stimuli (Fig 7C & 7D). These results indicate that during ongoing activ-
ity, ER-mediated Ca^{2+} disruptions drive a competition between the primary modes of ex-
ocytosis; short-lived synchronous release that dominates evoked release during low-fre-
quency stimulation, and slower asynchronous release which persists for several millisec-
onds and builds up during higher-frequency stimuli trains [69, 39]. Consistent with pre-
vious reports, we observe that during the pulse-train depression, synchronous release
progressively declines, whereas asynchronous release peaks and subsequently decays
with stimulus number (Fig 7G & 7H). These results also show that while both forms of
release compete for the same pool of releasable vesicles, residual Ca^{2+}, which builds up
during repetitive stimulation may allow asynchronous release access to a larger subset of
the RRP initially [44, 45, 102]. Our findings here indicate that impairments such as FAD
pathology, which trigger elevated levels of residual intracellular $[Ca^{2+}]$ (Fig 7F), signifi-
cantly enhance asynchronous release during first few pulses (Fig 7G). For both WT and
FAD-affected synapses, the decrease in asynchronous release after the peak is dictated by
competition with synchronous release for the same vesicle resources, which are rapidly
depleted with subsequent stimuli (Fig 7G & 7H) [45, 103]. Interestingly, the greater degree
of depression in the FAD-affected synapse is positively correlated with profound increase
and decrease in the rates of asynchronous and synchronous release respectively. Together,
our data suggest that during the stimulus train, AD pathology elicits significantly more
asynchronous release at the expense of synchronous release, consistent with the notion
that elevated residual Ca^{2+} underlies asynchronous release. Since the majority of evoked
exocytosis occurs synchronously with AP-triggered Ca^{2+} influx, the enhanced switch from
synchronous to asynchronous release in FAD-affected synapses reflect the increased de-
pression of synaptic transmission with repetitive stimulation. As clear from Supplemen-
tary Fig 4, the higher coupling between the microdomain around IP3Rs cluster and AZ
exacerbate the synaptic depression in AD-affected synapses more than WT synapses.

623
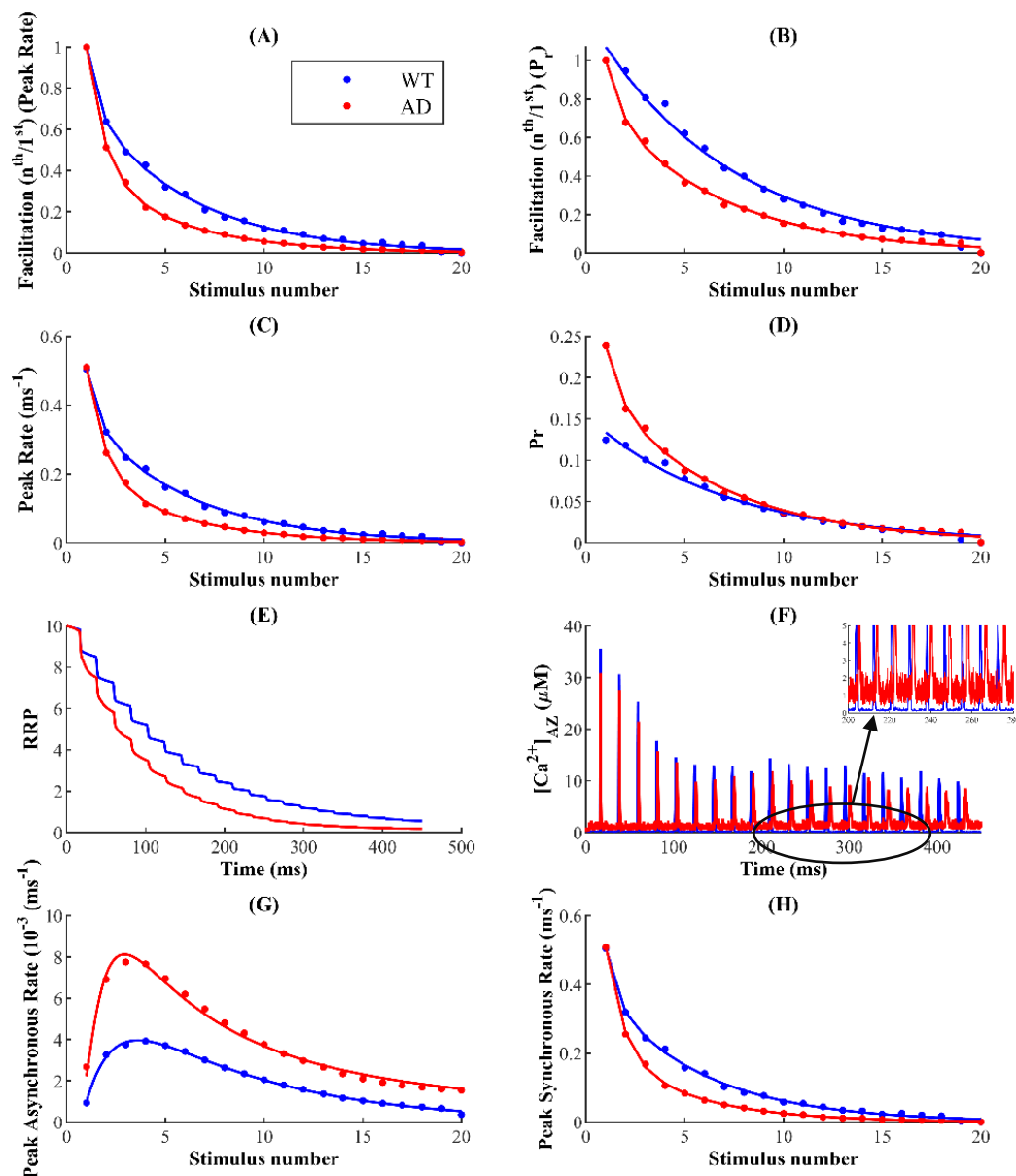
Figure 7. The AD-affected synapse exhibit stronger depression in response to 20 pulse stimulus-train delivered at 20 Hz: Facilitation obtained from peak rate (**A**) and P_r (**B**) shows that AD pathology induces more severe depression relative to control conditions. Peak release rate (**C**) and P_r (**D**) following each AP in the train. (**E**) Pulse train depression is primarily governed by RRP depletion, which is more severe in synapses with AD pathology. (**F**) $[Ca^{2+}]_{AZ}$ (top) and zoom-in (inset) showing the differences in basal $[Ca^{2+}]_{AZ}$ levels. (**G**) Asynchronous release peaks and subsequently decays following depletion of RRP. (**H**) Peak synchronous release mimics the response seen in the overall release.

624
625
626
627
628
629
630
631

632

633

3.4. Synchrony of release events is reduced in FAD-affected synapses 634

Motivated by substantial evidence supporting reduced temporal coordination of 635
neural activity in AD-affected networks, we next examine the degree of synchronization 636
between stimulus and response in WT and AD-affected synapses during repetitive stim- 637
ulation [104—106]. Given the loose temporal coordination of neuronal response during 638
asynchronous release, the observed shift from synchronous to asynchronous release dur- 639
ing stimulation in FAD should reduce the synchrony between the pulse and response [45]. 640
To test this hypothesis, we measure the event synchrony between each spike in the pulse 641
train and corresponding release using a modified Pinsky-Rinzel algorithm (see Methods 642
for details) [73, 74]. In extreme cases, pulse and release event times can either be perfectly 643
aligned with synchrony value of 1, reflecting pristine temporal stimulus-response coordi- 644
nation, or desynchronized where synchrony value of 0 reflects temporally uncorrelated 645
activity and stimulus patterns. 646

The phase of individual release events in response to a stimulus train reveals that 647
synapses with FAD pathology exhibit significant decrease in coherence of stimulus and 648
release events, an observation that is seen consistently across a wide range of the P_r values 649
(Fig 8A & B). In-silico studies of the effect of presynaptic Ca^{2+} stores on exocytosis at the 650
CA3 terminal suggest that the ER allows highly stochastic hippocampal synapses with 651
low intrinsic release probability to operate with increased reliability [93]. Unsurprisingly, 652
in both the diseased and WT cases, synapses with low P_r exhibit relatively higher phase 653
coherence that persists upon subsequent stimulation (Fig 8A & B). Thus, our findings here 654
suggest that the alternative strategy to achieve robust firing rates—employed by synapses 655
with high intrinsic P_r that deplete the RRP quickly—may render the synapses unreliable 656
during repetitive stimulation. 657

658
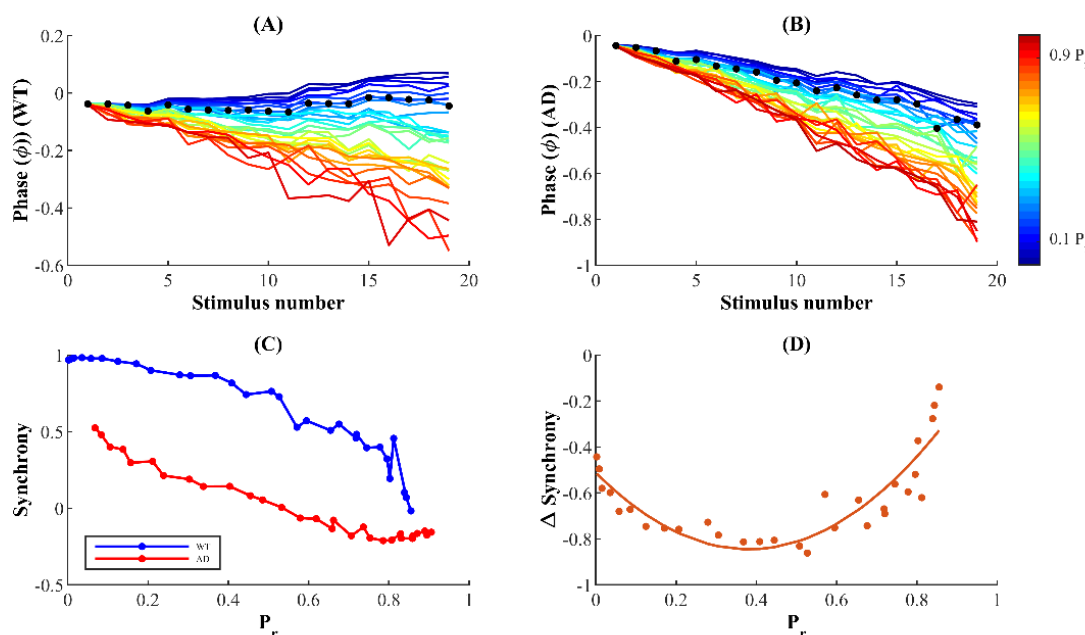
Figure 8. AD-related Ca^{2+} disruptions impair spike-SVR synchrony: The phase of individual release 659
events with respect to AP in WT (**A**) and AD-affected (**B**) synapses over a wide range of P_r values. 660
Black dots indicate the event phases corresponding to 35 VGCCs with initial P_r during pulse train 661
(P_{rI}) equal to 0.14; (C) Synchrony of release event in response to the preceding pulse in WT and AD- 662
affected synapses; (D) The magnitude of relative synchrony change from WT to AD conditions as a 663
function of initial release probability during prolonged stimulation. 664

Furthermore, a quantitative comparison of the synchrony measure reveals that FAD- 665
affected synapses with altered intracellular Ca^{2+} signaling exhibit significantly reduced 666

temporal coordination of activity as compared to WT synapses. This suggests that in addition to other impairments discussed above, unreliability in the temporal coordination of neuronal activity is likely also a hallmark of FAD-affected synaptic terminals (Fig 8C). This conclusion is consistent with *in vivo* recordings from neocortical pyramidal neurons where amyloid-β plaques in APP-Sw (Tg2576 transgenic mice model of AD) increased jitter in evoked AP, consequently reducing synaptic integration and information transfer [107]. Although our data so far indicate that synapses with higher P_r express reduced synchronization in both WT and FAD conditions, the relative sensitivity of synapses with low, intermediate, and high P_r to pathological alternations is yet to be explored. Thus, we next examine the relative change in synchrony from WT to FAD condition across a wide range of P_r values (Fig 8D). Our results show that there is an inverted bell-shaped relationship between relative synchrony and intrinsic P_r, suggesting that the physiological (intermediate) P_r which allows small hippocampal synapses to operate with reliable firing rates may also renders them more sensitive to pathological alterations. Taken together, these data suggest that the pathophysiological manifestations of impaired intracellular Ca^{2+} handling include suboptimal neuronal synchronization, reducing the fidelity of information integration and transmission. In addition, the results confirm that hippocampal synapses with intermediate P_r values exhibit a more severe impairment of their otherwise finely tuned temporal rate codes when subject to FAD-related alterations in Ca^{2+} signaling.

4. Discussion

Despite extensive experimental studies reporting the ubiquitous presence of ER in both axonal and dendritic compartments of neurons, little is known about its role in modifying major components of synaptic transmission during AD related pathologies [23, 108, 109]. In this study, we fill this gap by building a detailed biophysical model that accurately captures the compartmentalized signaling of Ca^{2+} at axonal terminals. In particular, our model incorporates ER-driven and AP-triggered presynaptic Ca^{2+} signaling as well as the resulting release mechanism in WT and FAD-affected synapses. This is especially motivated by reports of distinct regulatory mechanisms for intracellular Ca^{2+}, which primarily includes a cluster of ligand-gated IP_3R Ca^{2+} channels situated on the ER as well as voltage activated Ca^{2+} channels constrained to the AZ, that result in tight microdomain signaling [47, 53, 56, 71, 110]. In hippocampal synapses, the formation of evoked transient Ca^{2+} microdomains in the AZ is predominantly mediated by the rapid kinetics of P/Q-type VGCCs which open with minimal delay upon the arrival of AP, while subcellular domains in the vicinity of the ER occurs via the stochastic gating of IP_3Rs that require IP_3 and Ca^{2+} binding. In order to make meaningful quantitative predictions, we proceeded by developing a model that accurately captures the characteristic IP_3R's gating in WT and FAD-affected neurons [18, 19, 21]. We next incorporated a comprehensive description of presynaptic processes including evoked Ca^{2+} influx through VGCCs; Ca^{2+} release and uptake by the ER; and synchronous, asynchronous, and spontaneous modes of synaptic transmission. Inspired by several lines of evidence elucidating the existence of a bidirectional interaction of intracellular Ca^{2+} channels and presynaptic VGCCs mediated by stromal interaction molecules (STIM-1) and Orai channels, we have implemented a bi-directional coupling between the ER and AZ in our model that uncovers a unique biphasic dependence of decay times of release and Ca^{2+} on the baseline probability [91, 111]. Our model incorporates these critical components of presynaptic signaling and especially reproduced the observed spatiotemporal characteristics of intracellular Ca^{2+}—rise times, decay times, and amplitudes of corresponding events—and accounts for the stochasticity of presynaptic Ca^{2+} dynamics driven by stochastic channel openings [18, 53, 67, 112]. Release rate, facilitation and depression varies dramatically among phasic and tonic synapses—phasic synapses are dominated by depression, whereas tonic synapses can facilitate tremendously by vesicle recruitment [24, 68]. Constrained by kinetics data of vesicular release observed in other phasic cell types, our model closely reproduces essential determinants of neurotransmitter release, which consequently promoted close estimation of PPR and

facilitation requirements necessary to maintain normal plasma membrane function [24, 72, 94]. Following these independent validations, it is reasonable to assume that the biophysical model and protocols developed in this work are physiologically realistic representation of neuronal processes in control and disease cases.

Broadening of Ca^{2+} waveforms and response profiles affect the reliability of synaptic information transfer at affected terminals. Our results suggest that FAD-associated increase in Ca^{2+} release from the ER affect nearly all aspects of SVR. Despite the high stochasticity at the hippocampal CA3 terminal, the ER allows individual synapses operating in the low- and intermediate-probability regime maintain relatively higher reliability of information-rate coding [93]. Here, our results show that the FAD-associated enhanced Ca^{2+} selectively diminishes the reliability of intermediate-P_r synapses, suggesting that low- and intermediate P_r synapses are more susceptible to FAD-associated Ca^{2+} disruptions. Importantly, the model predicts that aberrant Ca^{2+} rise in AD-affected neurons may trigger hyperactivity over very short timescales (~30-60 msec) and lowers facilitation during prolonged (~450 msec) stimulation. We also report enhanced excitability in pathological synapses when simulated with higher coupling, which corresponds to a tighter feedback loop between the ER and AZ. Thus, our findings here provide a plausible explanation for why alterations in ER Ca^{2+} handling, which result in excessive efflux, induce a severe perturbation of neuronal processes that can in turn decrease the reliability of information encoded in the firing rate of neurons affected by FAD pathology [93, 113]. Overall, our findings provide novel insights into the role of aberrant ER Ca^{2+} release in altering the release profile of a synapse in AD and other neurodegenerative diseases where such Ca^{2+} impairments are observed [114].

Many explorations into the Ca^{2+}-dependence of release have proposed that periodic Ca^{2+} release from the ER, which occurs predominantly via the rapid gating kinetics of IP$_3$R, could trigger a series of physiological events—such as activating Ca^{2+}-sensing G proteins—that eventually manifest as changes in the global [Ca^{2+}] and, in turn, influence spontaneous release: a miniature form of exocytosis [28, 29]. Although IP$_3$Rs are differentially expressed according to cell type, several studies report the functional involvement of IP$_3$Rs in sculpting long-term potentiation (LTP) or depression (LTD) profiles in the CA1 region of the hippocampus [115, 116]. In particular, immunocytochemical evidence reveals the expression of IP$_3$Rs in presynaptic terminals of the rat CA3-CA1 hippocampal synapses and elucidates their modulatory role in presynaptic neurotransmitter release and synaptic plasticity [109]. Shorter opening times and longer closing times are characteristic features of the gating kinetics of IP$_3$Rs in cortical neurons and are essential for the homeostasis of local and global Ca^{2+} in the norm. Consistent with these requirements, studies on AD patients have implicated exaggerated Ca^{2+} release mediated by altered IP$_3$R activity to dysregulation of bulk Ca^{2+} which consequently triggers progressive loss of synaptic function [117—120]. From our model it is clear that these intrinsic biophysical properties of IP$_3$R make it highly effective at maintaining physiological bulk Ca^{2+} and P_r, whereas upregulated IP$_3$R orchestrates exaggerated Ca^{2+} from the ER and in turn increases the P_r.

Consistent with experimental evidence, our model reproduces the well-established inverse relationship between the P_r and PPR but suggests that the enhanced STP over rapid timescales observed in FAD merely indicates hyperactivity rather than increased synaptic reliability [72, 121]. The most crucial insight from this finding is that pathological synapses retain a longer history of Ca^{2+} dynamics, which consequently causes them to exhibit enhanced excitation in a paired-pulse protocol. The traditional view claiming the massive reduction in the efficacy of excitatory synaptic transmission in early stages of AD has been challenged recently by several studies reporting aberrant Ca^{2+} homeostasis and hyperactivity in AD-affected neuronal networks [84, 100, 101]. A key finding of these studies is that hyperactivity is an early dysfunction in hippocampal synapses, whereas neuronal silencing emerges during later stages of the disease. Our model predicts that synap-

tic facilitation and depression depend on the timescale and frequency of stimulation. Relatively short low-frequency stimuli cause facilitation, which supports the idea that by enhancing potentiating over rapid time scales, aberrant Ca^{2+} release from intracellular stores plays an important role in the history-dependent neuronal hyperactivity observed during early states of FAD.

Our model shows that long high-frequency pulses trigger depression in FAD-affected synapses, which is governed by depletion of RRP of vesicles. Experimental evidence reports three distinct molecular pathways for exocytosis [39]. Indeed, synchronous, asynchronous, and spontaneous modes of vesicular release, characterized by distinct release timescales, have been reported in cultured hippocampal synaptic terminals [28, 44]. Synaptotagmin-1 (Syt1) and 7 (Syt7) are the Ca^{2+} sensors controlling the timescales of synchronous and asynchronous release in CA3 pyramidal neurons respectively [39, 122]. The rapid kinetics and low Ca^{2+} affinity of Syt1 satisfies the remarkable temporal precision of synchronous release, where most vesicles immediately fuse with the membrane following stimulation. On the other hand, the slow kinetics of Syt7 promotes progressive desynchronization of release later in the spike train [123]. Studies on Syt1 knockout mice reported selective abolishment of synchronous release and increase in the magnitude of asynchronous release. Likewise, knockdown of Syt7 enhanced synchronous release in zebrafish's neuromuscular junction, suggesting that the primary modes of exocytosis draw from the same vesicle resources in the RRP, which causes their activity patterns to be negatively correlated [40, 44, 123—126]. The most critical insight of these findings is that manipulations that suppress synchronous release increases the vesicle resources available for asynchronous release and indirectly enhance its magnitude. In agreement with the above, during ongoing activity, we observed a shift from synchronous to asynchronous exocytosis leading to increased depression of synaptic transmission during FAD pathology.

CA3-CA1 presynaptic terminals are equipped with a conspicuously low release probability that allows them to maintain a delicate balance between facilitation and reliability, giving rise to finely tuned rate codes with remarkable temporal precision. Thus, perturbations of release mechanisms are expected to alter the fidelity of neural rhythms in AD. Indeed, cortical neurons with Aβ peptide expressed reduced N-methyl D-aspartate (NMDA) receptor density, resulting in rapid and persistent depression of NMDA-evoked currents [106]. Moreover, the severe impairment of evoked synaptic response latency observed in Tg2576 mice overexpressing APP provides direct evidence for reduced temporal coincidence of response in AD [107]. These findings suggest that impaired response precision is an acute effect of perturbations due to AD that leads to overt cortical deficits. In agreement with these observations, our results reveal increased latency of release events in FAD and uncover unique dependence of synchrony change—from control to FAD—on intrinsic Pr. The loss in temporal coordination of release in FAD is more severely expressed at a physiologically plausible P_r range for hippocampal synapses, although lower-P_r synapses exhibit relatively elevated temporal precision in both WT and FAD-affected synapses. Thus, despite the high fidelity of hippocampal synapses, their conspicuously low response success may make them more susceptible to AD pathology. We hope that future experiments will uncover the molecular mechanisms underlying the pathological enhancement of susceptibility in low-P_r hippocampal synapses.

We remark that while our model is developed to be consistent with most observations in the hippocampal CA3-CA1 synapses, it does not incorporate the uneven distribution of P/Q-type, N-type and R-type VGCCs specifically found in the AZ of central synapses [66, 127]. At hippocampal glutamatergic synapses, Cav2.1—P/Q-type—channels are thought to be most enriched at the presynaptic AZ and predominantly govern Ca^{2+} influx at the axon terminal [52]. Thus, like others, we value parsimony and use a formulation with only P/Q VGCCs [67]. Furthermore, results from cultured hippocampal and superior cervical ganglion neurons provide evidence for direct interactions between the release machinery and VGCCs, implying that channel distribution is important for accurately predicting the spatiotemporal profiles of evoked release [128, 129]. Our model does not

capture the effect of spatial distribution of VGCCs on synaptic transmission, neither does it incorporate other mechanisms for paired-pulse modulation expressed at putative single hippocampal synapses—lateral inhibition and release inactivation [72, 94]. Thus, despite reproducing the observed inverse relationship between paired-pulse facilitation and initial P_r, our model falls short of the measured values, suggesting that we cannot eliminate additional mechanisms when investigating the interplay between residual Ca^{2+}, facilitation, and depression. Although IP_3R-dependent modulation of cytosolic Ca^{2+} is usually adequate for explaining the critical aspects of ER Ca^{2+} release and regulation of neurotransmission, the upregulation of RyR expression and modulation of IP_3Rs' gating due to Ca^{2+} release through RyRs (and vice versa) are also thought to play a key role in the aberrant Ca^{2+} release from the ER, as well as propagation of presynaptic signals [10—22, 130]. It has been suggested that at the hippocampal Schaffer-collateral pathway, presynaptic presenilin inactivation perturbs STP and facilitation via impaired RyR function [36, 131]. Furthermore, in 3xTg-AD mice, deviant RyR activity triggers Ca^{2+} signaling alterations that promote synaptic depression [37]. However, our model does not describe the contribution of presynaptic RyRs to vesicular release, as the biophysical properties of these receptors yield a distinct temporal range of Ca^{2+} transients that can modulate LTP/LTD [132, 133]. Presenilin mutations account for a significant portion of FAD cases, however, our current model does not incorporate ER-resident Ca^{2+} permeable leak channels formed by Presenilins that are disrupted in FAD affected neurons [134]. Another key factor missing from our model is synaptic mitochondria. Mitochondria play a key role in shaping Ca^{2+} gradients in synaptic terminals. Synaptic mitochondria are among the earliest targets in AD. Among other things, the ATP production and Ca^{2+} buffering capacities of mitochondria are severely disrupted [135, 136]. All these issues are the subjects of our future research.

In summary, we have leveraged diverse experimental data to model Ca^{2+} homeostasis in axonal terminal and how exocytosis is affected in FAD. Motivated by the difficulty in probing signaling cascades at the AZ of small hippocampal synapses, our main goal was to build a comprehensive but simple framework for unravelling the role of enhanced Ca^{2+} release from the ER in SVR during FAD pathology. In addition to agreeing closely with several observations about the kinetics of IP_3Rs, SVR, and synaptic plasticity in both WT and diseased synapses, our modelling work provides key insights into impaired presynaptic function in FAD. Specifically, we make five key predictions:

1. The overall P_r in response to a single AP is upregulated in FAD-affected synapses;
2. Short-lived low-frequency stimuli promotes potentiation in FAD-affected synapses;
3. During sustained high-frequency stimulation, FAD-affected terminals exhibit enhanced depression;
4. FAD-affected synapses operate less reliably and;
5. The effect of FAD pathology is exacerbated in synapses with low to intermediate P_r.

Although extensive experimental evidence corroborates our findings and demonstrates the significance of ER Ca^{2+} dysregulation and loss of synaptic integrity in FAD, SVR therapeutics remain underdeveloped. For example, the current lack of validated *in vivo* biomarkers that can be used as proxies of synaptic dysfunction has directed most translational efforts towards indirect measures of synaptic integrity in AD [137]. Our findings suggest that targeting essential components of neurotransmission as well as related pathways of the ER could potentially aid biomarker identification and drug discovery efforts in FAD. In future research, we expect to incorporate a better and comprehensive understanding of the mechanisms underlying neuronal Ca^{2+} dysregulation to provide better insights into the disease pathogenesis and therapeutic directions. Taken together with the aforementioned limitations, our analysis highlights the need for further studies on investigating the role of perturbed Ca^{2+} signaling due to intracellular organelles such as the ER

and mitochondria in cognitive deficits associated with AD and other neurodegenerative diseases.

Institutional Review Board Statement: Not applicable.

Informed Consent Statement: Not applicable

Data Availability Statement: The complete model code as well as analysis scripts will be posted on our lab's webpage after the manuscript is accepted for publication.

Conflicts of Interest: The authors declare no conflict of interest.

References

1. Ferri, C. P.; Prince, M.; Brayne, C.; Brodaty, H.; Fratiglioni, L.; Ganguli, M.; Hall, K.; Hasegawa, K.; Hendrie, H.; Huang, Y.; et al. Global prevalence of dementia: a Delphi consensus study. The Lancet 2005, 366 (9503), 2112–2117 DOI: 10.1016/s0140-6736(05)67889-0

2. Reitz, C.; Mayeux, R. Alzheimer disease: Epidemiology, diagnostic criteria, risk factors and biomarkers. Biochemical Pharmacology 2014, 88 (4), 640–651 DOI: 10.1016/j.bcp.2013.12.024.

3. Cerejeira, J.; Lagarto, L.; Mukaetova-Ladinska, E. B. (2012). Behavioral and psychological symptoms of dementia. Frontiers in neurology, 2012, 3, 73. https://doi.org/10.3389/fneur.2012.00073

4. Selkoe, D. J. Alzheimer's Disease Is a Synaptic Failure. Science 2002, 298(5594), 789–791 DOI: 10.1126/science.1074069

5. Sims, R.; Hill, M.; Williams, J.. The multiplex model of the genetics of Alzheimer's disease. Nature Neuroscience 2020, 23 (3), 311–322 DOI: 10.1038/s41593-020-0599-5.

6. Mondragón-Rodríguez, S.; Basurto-Islas, G.; Santa-Maria, I.; Mena, R.; Binder, L. I.; Avila, J.; Smith, M. A.; Perry, G.; García-Sierra, F. Cleavage and conformational changes of tau protein follow phosphorylation during Alzheimer's disease. International Journal of Experimental Pathology 2008, 89 (2), 81–90 DOI: 10.1111/j.1365-2613.2007.00568.x.

7. Geula, C.; Mesulam, M.-M.; Saroff, D. M.; Wu, C.-K. Relationship Between Plaques, Tangles, and Loss of Cortical Cholinergic Fibers in Alzheimer Disease. Journal of Neuropathology & Experimental Neurology 1998, 57 (1), 63–75 DOI: 10.1097/00005072-199801000-00008.

8. Vogt, L. J. K.; Hyman, B. T.; Van Hoesen, G. W.; Damasio, A. R. Pathological alterations in the amygdala in Alzheimer's disease. Neuroscience 1990, 37 (2), 377–385 DOI: 10.1016/0306-4522(90)90408-v.

9. Hyman, B.T., Van Horsen, G.W., Damasio, A.R., & Barnes, C.L. Alzheimer's disease: cell-specific pathology isolates the hippocampal formation. Science 1984, 225, 1168–1170 DOI: 10.1126/science.6474172

10. Ferreiro, E.; Oliveira, C. R.; Pereira, C. Involvement of endoplasmic reticulum Ca2+ release through ryanodine and inositol 1,4,5-triphosphate receptors in the neurotoxic effects induced by the amyloid-? peptide. Journal of Neuroscience Research 2004, 76 (6), 872–880 DOI: 10.1002/jnr.20135.

11. Kuchibhotla, K. V.; Goldman, S. T.; Lattarulo, C. R.; Wu, H.-Y.; Hyman, B. T.; Bacskai, B. J. Aβ Plaques Lead to Aberrant Regulation of Calcium Homeostasis In Vivo Resulting in Structural and Functional Disruption of Neuronal Networks. Neuron 2008, 59 (2), 214–225 DOI: 10.1016/j.neuron.2008.06.008.

12. Liang, J.; Kulasiri, D.; Samarasinghe, S. Ca2+ dysregulation in the endoplasmic reticulum related to Alzheimer's disease: A review on experimental progress and computational modeling. Biosystems 2015, 134, 1–15 DOI: 10.1016/j.biosystems.2015.05.003.

13. Plácido, A. I.; Pereira, C. M. F.; Duarte, A. I.; Candeias, E.; Correia, S. C.; Santos, R. X.; Carvalho, C.; Cardoso, S.; Oliveira, C. R.; Moreira, P. I. The role of endoplasmic reticulum in amyloid precursor protein processing and trafficking: Implications for Alzheimer's disease. Biochimica et Biophysica Acta (BBA) - Molecular Basis of Disease 2014, 1842 (9), 1444–1453 DOI: 10.1016/j.bbadis.2014.05.003.

14. Renner, M.; Lacor, P. N.; Velasco, P. T.; Xu, J.; Contractor, A.; Klein, W. L.; Triller, A. Deleterious Effects of Amyloid β Oligomers Acting as an Extracellular Scaffold for mGluR5. Neuron 2010, 66 (5), 739–754 DOI: 10.1016/j.neuron.2010.04.029

15. Demuro, A.; Parker, I. Cytotoxicity of Intracellular A 42 Amyloid Oligomers Involves Ca2+ Release from the Endoplasmic Reticulum by Stimulated Production of Inositol Trisphosphate. The Journal of Neuroscience 2013, 33 (9), 3824–3833 DOI: 10.1523/jneurosci.4367-12.2013.

16. Del Prete, D.; Checler, F.; Chami, M. Ryanodine receptors: physiological function and deregulation in Alzheimer disease. Molecular Neurodegeneration 2014, 9 (1), 21 DOI: 10.1186/1750-1326-9-21.

17. Khachaturian, Z. S. Calcium Hypothesis of Alzheimer's disease and brain aging: A framework for integrating new evidence into a comprehensive theory of pathogenesis. Alzheimer's & Dementia 2017, 13 (2), 178 DOI: 10.1016/j.jalz.2016.12.006.

18. Mak, D.-O. D.; Cheung, K.-H.; Toglia, P.; Foskett, J. K.; Ullah, G. Analyzing and Quantifying the Gain-of-Function Enhancement of IP3 Receptor Gating by Familial Alzheimer's Disease-Causing Mutants in Presenilins. PLOS Computational Biology 2015, 11 (10), e1004529 DOI: 10.1371/journal.pcbi.1004529.

19. Cheung, K.-H.; Shineman, D.; Müller, M.; Cárdenas, C.; Mei, L.; Yang, J.; Tomita, T.; Iwatsubo, T.; Lee, V. M.-Y.; Foskett, J. K. Mechanism of Ca2+ Disruption in Alzheimer's Disease by Presenilin Regulation of InsP3 Receptor Channel Gating. Neuron 2008, 58 (6), 871–883 DOI: 10.1016/j.neuron.2008.04.015.

20. Demuro, A.; Mina, E.; Kayed, R.; Milton, S. C.; Parker, I.; Glabe, C. G. Calcium Dysregulation and Membrane Disruption as a Ubiquitous Neurotoxic Mechanism of Soluble Amyloid Oligomers*♦. Journal of Biological Chemistry 2005, 280 (17), 17294–17300 DOI: 10.1074/jbc.m500997200.

21. Cheung, K.-H.; Mei, L.; Mak, D.-O. D.; Hayashi, I.; Iwatsubo, T.; Kang, D. E.; & Foskett, J. K. Gain-of-Function Enhancement of IP 3 Receptor Modal Gating by Familial Alzheimer's Disease–Linked Presenilin Mutants in Human Cells and Mouse Neurons. Science Signaling 2010, 3(114), ra22–ra22. DOI: 10.1126/scisignal.2000818

22. Stutzmann, G. E. Enhanced Ryanodine Receptor Recruitment Contributes to Ca2+ Disruptions in Young, Adult, and Aged Alzheimer's Disease Mice. The Journal of Neuroscience 2006, 26 (19), 5180–5189 DOI: 10.1523/jneurosci.0739-06.2006.

23. Mattson, M. P.; Laferla, F. M.; Chan, S. L.; Leissring, M. A.; Shepel, P. N.; Geiger, J. D. Calcium signaling in the ER: its role in neuronal plasticity and neurodegenerative disorders. Trends in Neurosciences 2000, 23 (5), 222–229 DOI: 10.1016/s0166-2236(00)01548-4.

24. Neher, E.; Sakaba, T. Multiple Roles of Calcium Ions in the Regulation of Neurotransmitter Release. Neuron 2008, 59 (6), 861–872 DOI: 10.1016/j.neuron.2008.08.019.

25. Zucker, R. S.; Regehr, W. G. Short-Term Synaptic Plasticity. Annual Review of Physiology 2002, 64 (1), 355–405 DOI: 10.1146/annurev.physiol.64.092501.114547.

26. Groffen, A. J.; Martens, S.; Arazola, R. D.; Cornelisse, L. N.; Lozovaya, N.; De Jong, A. P. H.; Goriounova, N. A.; Habets, R. L. P.; Takai, Y.; Borst, J. G.; Brose, N.; Mcmahon, H. T.; & Verhage, M. Doc2b Is a High-Affinity Ca2+ Sensor for Spontaneous Neurotransmitter Release. Science 2010, 327(5973), 1614–1618. DOI: 10.1126/science.1183765

27. Eggermann, E.; Bucurenciu, I.; Goswami, S. P.; Jonas, P. Nanodomain coupling between Ca2+ channels and sensors of exocytosis at fast mammalian synapses. Nature Reviews Neuroscience 2012, 13 (1), 7–21 DOI: 10.1038/nrn3125.

28. Emptage, N. J.; Reid, C. A.; Fine, A. Calcium Stores in Hippocampal Synaptic Boutons Mediate Short-Term Plasticity, Store-Operated Ca2+ Entry, and Spontaneous Transmitter Release. Neuron 2001, 29 (1), 197–208 DOI: 10.1016/s0896-6273(01)00190-8.

29. Vyleta, N. P.; Smith, S. M. Spontaneous Glutamate Release Is Independent of Calcium Influx and Tonically Activated by the Calcium-Sensing Receptor. The Journal of Neuroscience 2011, 31 (12), 4593–4606 DOI: 10.1523/jneurosci.6398-10.2011.

30. Bouchard, R.; Pattarini, R.; Geiger, J. D. Presence and functional significance of presynaptic ryanodine receptors. Progress in Neurobiology 2003, 69 (6), 391–418 DOI: 10.1016/s0301-0082(03)00053-4.

31. Shepherd, G. M. G.; Harris, K. M. Three-Dimensional Structure and Composition of CA3→CA1 Axons in Rat Hippocampal Slices: Implications for Presynaptic Connectivity and Compartmentalization. The Journal of Neuroscience 1998, 18 (20), 8300–8310 DOI: 10.1523/jneurosci.18-20-08300.1998.

32. Sharp, A.; Mcpherson, P.; Dawson, T.; Aoki, C.; Campbell, K.; Snyder, S. Differential immunohistochemical localization of inositol 1,4,5- trisphosphate- and ryanodine-sensitive Ca2+ release channels in rat brain. The Journal of Neuroscience 1993, 13 (7), 3051–3063 DOI: 10.1523/jneurosci.13-07-03051.1993.

33. Bardo, S.; Cavazzini, M. G.; Emptage, N. The role of the endoplasmic reticulum Ca2+ store in the plasticity of central neurons. Trends in Pharmacological Sciences 2006, 27 (2), 78–84 DOI: 10.1016/j.tips.2005.12.008.

34. Chen, M.; Van Hook, M. J.; Thoreson, W. B. Ca2+ Diffusion through Endoplasmic Reticulum Supports Elevated Intraterminal Ca2+ Levels Needed to Sustain Synaptic Release from Rods in Darkness. The Journal of Neuroscience 2015, 35 (32), 11364–11373 DOI: 10.1523/jneurosci.0754-15.2015.

35. Chen, M.; Križaj, D.; & Thoreson, W.B. Intracellular calcium stores drive slow non-ribbon vesicle release from rod photoreceptors. Front. Cell. Neurosci. 2014, 8, 20 DOI: 10.3389/fncel.2014.00020

36. Zhang, C.; Wu, B.; Beglopoulos, V.; Wines-Samuelson, M.; Zhang, D.; Dragatsis, I.; Südhof, T. C.; Shen, J. Presenilins are essential for regulating neurotransmitter release. Nature 2009, 460 (7255), 632–636 DOI: 10.1038/nature08177.

37. Chakroborty, S.; Kim, J.; Schneider, C.; Jacobson, C.; Molgo, J.; Stutzmann, G. E. Early Presynaptic and Postsynaptic Calcium Signaling Abnormalities Mask Underlying Synaptic Depression in Presymptomatic Alzheimer's Disease Mice. The Journal of Neuroscience 2012, 32 (24), 8341–8353 DOI: 10.1523/jneurosci.0936-12.2012.

38. Neves, G.; Cooke, S. F.; Bliss, T. V. P. Synaptic plasticity, memory and the hippocampus: a neural network approach to causality. Nature Reviews Neuroscience 2008, 9 (1), 65–75 DOI: 10.1038/nrn2303.

39. Kaeser, P. S.; Regehr, W. G. Molecular Mechanisms for Synchronous, Asynchronous, and Spontaneous Neurotransmitter Release. Annual Review of Physiology 2014, 76 (1), 333–363 DOI: 10.1146/annurev-physiol-021113-170338.

40. Geppert, M.; Goda, Y.; Hammer, R. E.; Li, C.; Rosahl, T. W.; et al. Synaptotagmin I: a major Ca2+ sensor for transmitter release at a central synapse. Cell. 1994, 79, 717–727. DOI: 10.1016/0092-8674(94)90556-8

41. Xu, J.; Mashimo, T.; Südhof, T. C. Synaptotagmin-1, -2, and -9: Ca2+ Sensors for Fast Release that Specify Distinct Presynaptic Properties in Subsets of Neurons. Neuron 2007, 54 (4), 567–581 DOI: 10.1016/j.neuron.2007.05.004.

42. Dodge, F. A. Jr.; Rahamimoff, R. On the relationship between calcium concentration and the amplitude of the end-plate potential. The Journal of physiology 1967, 189(2), 90–92. PMID: 6034150.

43. Sudhof, T. C. Calcium Control of Neurotransmitter Release. Cold Spring Harbor Perspectives in Biology 2012, 4 (1), a011353–a011353 DOI: 10.1101/cshperspect.a011353.

44. Hagler, D.J.; Goda, Y. Properties of synchronous and asynchronous release during pulse train depression in cultured hippocampal neurons. J. Neurophysiol 2001, 85, 2324–2334. https://doi.org/10.1152/jn.2001.85.6.2324

45. Yang, L.; Wang, B.; Long, C.; Wu, G.; Zheng, H. Increased asynchronous release and aberrant calcium channel activation in amyloid precursor protein deficient neuromuscular synapses. Neuroscience 2007, 149 (4), 768–778 DOI: 10.1016/j.neuroscience.2007.08.025.

46. Yamamoto, K.; Kobayashi, M. Opposite Roles in Short-Term Plasticity for N-Type and P/Q-Type Voltage-Dependent Calcium Channels in GABAergic Neuronal Connections in the Rat Cerebral Cortex. The Journal of Neuroscience 2018, 38 (46), 9814–9828 DOI: 10.1523/jneurosci.0337-18.2018.

47. Cao, P.; Tan, X.; Donovan, G.; Sanderson, M. J.; Sneyd, J. A Deterministic Model Predicts the Properties of Stochastic Calcium Oscillations in Airway Smooth Muscle Cells. PLOS Computational Biology 2014, 10 (8), e1003783 DOI: 10.1371/journal.pcbi.1003783.

48. Berridge, M. J.; Bootman, M. D.; Roderick, H. L. Calcium signaling: dynamics, homeostasis, and remodeling. Nature Reviews Molecular Cell Biology 2003, 4 (7), 517–529 DOI: 10.1038/nrm1155.

49. Keener, J.; Sneyd, J. Mathematical Physiology I: Cellular Physiology. 2nd ed. Springer Science + Business Media, LLC; 2009.

50. Dupont G, Falcke M, Kirk V, Sneyd J. Models of Calcium Signaling. Springer International Publishing Switzerland 2016.

51. Schikorski, T.; Stevens, C. F. Quantitative Ultrastructural Analysis of Hippocampal Excitatory Synapses. The Journal of Neuroscience 1997, 17 (15), 5858–5867 DOI: 10.1523/jneurosci.17-15-05858.1997.

52. Holderith, N.; Lorincz, A.; Katona, G.; Rózsa, B.; Kulik, A.; Watanabe, M.; Nusser, Z. Release probability of hippocampal glutamatergic terminals scales with the size of the active zone. Nature Neuroscience 2012, 15 (7), 988–997 DOI: 10.1038/nn.3137.

53. Ermolyuk, Y. S.; Alder, F. G.; Surges, R.; Pavlov, I. Y.; Timofeeva, Y.; Kullmann, D. M.; Volynski, K. E. Differential triggering of spontaneous glutamate release by P/Q-, N- and R-type Ca2+ channels. Nature Neuroscience 2013, 16 (12), 1754–1763 DOI: 10.1038/nn.3563.

54. Ohana, O.; Sakmann, B. Transmitter release modulation in nerve terminals of rat neocortical pyramidal cells by intracellular calcium buffers. The Journal of Physiology 1998, 513 (1), 135–148 DOI: 10.1111/j.1469-7793.1998.135by.x.

55. Rozov, A.; Burnashev, N.; Sakmann, B.; Neher, E. Transmitter release modulation by intracellular Ca 2+ buffers in facilitating and depressing nerve terminals of pyramidal cells in layer 2/3 of the rat neocortex indicates a target cell-specific difference in presynaptic calcium dy. The Journal of Physiology 2001, 531 (3), 807–826 DOI: 10.1111/j.1469-7793.2001.0807h.x.

56. Wang, L.-Y.; Augustine, G. J. Presynaptic nanodomains: a tale of two synapses. Frontiers in Cellular Neuroscience 2015, 8. DOI: 10.3389/fncel.2014.00455

57. Politi, A.; Gaspers, L. D.; Thomas, A. P.; Höfer, T. Models of IP3 and Ca2+ Oscillations: Frequency Encoding and Identification of Underlying Feedbacks. Biophysical Journal 2006, 90 (9), 3120–3133 DOI: 10.1529/biophysj.105.072249.

58. Minicucci, J.; Alfond, M.; Demuro, A.; Gerberry, D.; Latulippe, J. Quantifying the dose-dependent impact of intracellular amyloid beta in a mathematical model of calcium regulation in xenopus oocyte. PLOS ONE 2021, 16 (1), e0246116 DOI: 10.1371/journal.pone.0246116.

59. Riascos, D.; De Leon, D.; Baker-Nigh, A.; Nicholas, A.; Yukhananov, R.; Bu, J.; Wu, C.-K.; Geula, C. Age-related loss of calcium buffering and selective neuronal vulnerability in Alzheimer's disease. Acta Neuropathologica 2011, 122 (5), 565–576 DOI: 10.1007/s00401-011-0865-4.

60. Kook, S.-Y.; Jeong, H.; Kang, M. J.; Park, R.; Shin, H. J.; Han, S.-H.; Son, S. M.; Song, H.; Baik, S. H.; Moon, M.; et al. Crucial role of calbindin-D28k in the pathogenesis of Alzheimer's disease mouse model. Cell Death & Differentiation 2014, 21 (10), 1575–1587 DOI: 10.1038/cdd.2014.67.

61. Miguel, J. C.; Perez, S. E.; Malek-Ahmadi, M.; & Mufson, E. J. Cerebellar Calcium-Binding Protein and Neurotrophin Receptor Defects in Down Syndrome and Alzheimer's Disease. Frontiers in aging neuroscience, 2021, 13, 645334. DOI: 10.3389/fnagi.2021.645334

62. De Young, G. W., & Keizer, J. A single-pool inositol 1,4,5-trisphosphate-receptor-based model for agonist-stimulated oscillations in Ca2+ concentration. Proceedings of the National Academy of Sciences 1992, 89(20), 9895–9899. DOI: 10.1073/pnas.89.20.9895

63. Shuai, J.; Pearson, J. E.; Foskett, J. K.; Mak, D.-O. D.; Parker, I. A Kinetic Model of Single and Clustered IP3 Receptors in the Absence of Ca2+ Feedback. Biophysical Journal 2007, 93 (4), 1151–1162 DOI: 10.1529/biophysj.107.108795.

64. Ullah, G.; Daniel Mak, D.-O.; Pearson, J. E. A data-driven model of a modal gated ion channel: The inositol 1,4,5-trisphosphate receptor in insect Sf9 cells. Journal of General Physiology 2012, 140 (2), 159–173 DOI: 10.1085/jgp.201110753.

65. Kopell, N.; Börgers, C.; Pervouchine, D.; Malerba, P.; Tort, A. Gamma and Theta Rhythms in Biophysical Models of Hippocampal Circuits. In: Hippocampal Microcircuits: A computational Modeler's Resource Book, edited by Cutsuridis V, Graham B, Cobb S, Vida I. New York: Springer 2010, pp 423–457

66. Bischofberger, J.; Geiger, J. R. P.; Jonas, P. Timing and Efficacy of Ca2+Channel Activation in Hippocampal Mossy Fiber Boutons. The Journal of Neuroscience 2002, 22 (24), 10593–10602 DOI: 10.1523/jneurosci.22-24-10593.2002.

67. Nadkarni, S.; Bartol, T. M.; Sejnowski, T. J.; Levine, H. Modelling Vesicular Release at Hippocampal Synapses. PLOS Computational Biology 2010, 6 (11), e1000983 DOI: 10.1371/journal.pcbi.1000983.

68. Pan, B.; Zucker, R. S. A General Model of Synaptic Transmission and Short-Term Plasticity. Neuron 2009, 62 (4), 539–554 DOI: 10.1016/j.neuron.2009.03.025.

69. Sun, J.; Pang, Z. P.; Qin, D.; Fahim, A. T.; Adachi, R.; Südhof, T. C. A dual-Ca2+-sensor model for neurotransmitter release in a central synapse. Nature 2007, 450 (7170), 676–682 DOI: 10.1038/nature06308.

70. Goda, Y.; Stevens, C. F. Two components of transmitter release at a central synapse. Proceedings of the National Academy of Sciences 1994, 91(26), 12942–12946. DOI:10.1073/pnas.91.26.12942

71. Heine, M.; Heck, J.; Ciuraszkiewicz, A.; Bikbaev, A. Dynamic compartmentalization of calcium channel signalling in neurons. Neuropharmacology 2020, 169, 107556 DOI: 10.1016/j.neuropharm.2019.02.038.

72. Dobrunz, L. E.; Huang, E. P.; Stevens, C. F. Very short-term plasticity in hippocampal synapses. Proceedings of the national academy of sciences 1997, 94(26), 14843-14847. DOI:10.1073/pnas.94.26.14843

73. Pinsky, P. F.; Rinzel, J. Synchrony measures for biological neural networks. Biological Cybernetics 1995, 73 (2), 129–137 DOI: 10.1007/bf00204051.

74. Strogatz, S. H.; Mirollo, R. E. Stability of incoherence in a population of coupled oscillators. Journal of Statistical Physics 1991, 63 (3-4), 613–635 DOI: 10.1007/bf01029202.

75. Ullah, G.; Jung, P. Modeling the Statistics of Elementary Calcium Release Events. Biophysical Journal 2006, 90 (10), 3485–3495 DOI: 10.1529/biophysj.105.073460.

76. Greotti, E.; Capitanio, P.; Wong, A.; Pozzan, T.; Pizzo, P.; Pendin, D. Familial Alzheimer's disease-linked presenilin mutants and intracellular Ca2+ handling: A single-organelle, FRET-based analysis. Cell Calcium 2019, 79, 44–56 DOI: 10.1016/j.ceca.2019.02.005.

77. Leissring, M. A.; Paul, B. A.; Parker, I.; Cotman, C. W.; Laferla, F. M. Alzheimer's Presenilin-1 Mutation Potentiates Inositol 1,4,5-Trisphosphate-Mediated Calcium Signaling in Xenopus. Journal of Neurochemistry 2008, 72 (3), 1061–1068 DOI: 10.1111/j.1471-4159.1999.721061.x.

78. Lopez, J. R.; Lyckman, A.; Oddo, S.; Laferla, F. M.; Querfurth, H. W.; Shtifman, A. Increased intraneuronal resting [Ca2+] in adult Alzheimer's disease mice. Journal of Neurochemistry 2008, 105 (1), 262–271 DOI: 10.1111/j.1471-4159.2007.05135.x.

79. Sätzler, K.; Söhl, L. F.; Bollmann, J. H.; Borst, J. G. G.; Frotscher, M.; Sakmann, B.; Lübke, J. H. R. Three-Dimensional Reconstruction of a Calyx of Held and Its Postsynaptic Principal Neuron in the Medial Nucleus of the Trapezoid Body. The Journal of Neuroscience 2002, 22 (24), 10567–10579 DOI: 10.1523/jneurosci.22-24-10567.2002.

80. Eshra, A.; Schmidt, H.; Eilers, J.; Hallermann, S. Calcium dependence of neurotransmitter release at a high-fidelity synapse. eLife 2021, 10 DOI: 10.7554/elife.70408.

81. Delvendahl, I.; Weyhersmüller, A.; Ritzau-Jost, A.; Hallermann, S. Hippocampal and cerebellar mossy fibre boutons - same name, different function. The Journal of Physiology 2013, 591 (13), 3179–3188 DOI: 10.1113/jphysiol.2012.248294.

82. Otsu, Y.; Murphy, T. H. Miniature Transmitter Release: Accident of Nature or Careful Design? Science Signaling 2003, (211), p54. DOI: 10.1126/stke.2112003pe54

83. Murthy, V. N.; Stevens, C. F. Reversal of synaptic vesicle docking at central synapses. Nature Neuroscience 1999, 2 (6), 503–507 DOI: 10.1038/9149.

84. Busche, M. A.; Chen, X.; Henning, H. A.; Reichwald, J.; Staufenbiel, M.; Sakmann, B.; Konnerth, A. Critical role of soluble amyloid-β for early hippocampal hyperactivity in a mouse model of Alzheimer's disease. Proceedings of the National Academy of Sciences 2012, 109(22), 8740–8745. DOI: 10.1073/pnas.1206171109

85. Stutzmann, G.E.; Caccamo. A.; LaFerla, F. M.; & Parker, I. Dysregulated IP3 Signaling in Cortical Neurons of Knock-In Mice Expressing an Alzheimer's-Linked Mutation in Presenilin1 Results in Exaggerated Ca2+ Signals and Altered Membrane Excitability. The Journal of Neuroscience 2004, 24, 508–513 DOI: 10.1523/jneurosci.4386-03.2004

86. Zatti, G.; Burgo, A.; Giacomello, M.; Barbiero, L.; Ghidoni, R.; Sinigaglia, G.; Florean, C.; Bagnoli, S.; Binetti, G.; Sorbi, S.; et al. Presenilin mutations linked to familial Alzheimer's disease reduce endoplasmic reticulum and Golgi apparatus calcium levels. Cell Calcium 2006, 39 (6), 539–550 DOI: 10.1016/j.ceca.2006.03.002.

87. Berridge, M. J. Calcium hypothesis of Alzheimer's disease. Pflügers Archiv - European Journal of Physiology 2010, 459 (3), 441–449 DOI: 10.1007/s00424-009-0736-1.

88. Karagas, N. E.; Venkatachalam, K. Roles for the Endoplasmic Reticulum in Regulation of Neuronal Calcium Homeostasis. Cells 2019, 8(10), 1232. doi:10.3390/cells8101232

89. Collin, T.; Marty, A.; Llano, I. Presynaptic calcium stores and synaptic transmission. Current opinion in neurobiology 2005, 15(3), 275-281. DOI: 10.1016/j.conb.2005.05.003

90. Stanley, E. F. The calcium channel and the organization of the presynaptic transmitter release face. Trends in neurosciences 1997, 20(9), 404-409. DOI: 10.1016/s0166-2236(97)01091-6

91. De Juan-Sanz, J.; Holt, G. T.; Schreiter, E. R.; De Juan, F.; Kim, D. S.; Ryan, T. A. Axonal Endoplasmic Reticulum Ca2+ Content Controls Release Probability in CNS Nerve Terminals. Neuron 2017, 93 (4), 867–881.e6 DOI: 10.1016/j.neuron.2017.01.010.

92. Karagas, N. E.; Venkatachalam, K. Roles for the Endoplasmic Reticulum in Regulation of Neuronal Calcium Homeostasis. Cells 2019, 8(10), 1232. DOI: 10.3390/cells8101232

93. Singh, N.; Bartol, T.; Levine, H.; Sejnowski, T.; Nadkarni, S. Presynaptic endoplasmic reticulum regulates short-term plasticity in hippocampal synapses. Communications Biology 2021, 4 (1) DOI: 10.1038/s42003-021-01761-7.

94. Dobrunz, L. E.; Stevens, C. F. Heterogeneity of Release Probability, Facilitation, and Depletion at Central Synapses. Neuron 1997, 18(6), 995-1008. DOI: 10.1016/s0896-6273(00)80338-4

95. Debanne, D.; Guérineau, N. C.; Gähwiler, B. H.; Thompson, S. M. Paired-pulse facilitation and depression at unitary synapses in rat hippocampus: quantal fluctuation affects subsequent release. The journal of physiology 1996, 491(1), 163-176. DOI: 10.1113/jphysiol.1996.sp021204

96. Citri, A.; Malenka, R. C. Synaptic Plasticity: Multiple Forms, Functions, and Mechanisms. Neuropsychopharmacology 2008, 33(1), 18-41. DOI: 10.1038/sj.npp.1301559

97. Guo, D.; Li, C. Population rate coding in recurrent neuronal networks with unreliable synapses. Cognitive neurodynamics 2012, 6(1), 75-87. DOI: 10.1007/s11571-011-9181-x

98. Mark S. Goldman. Enhancement of Information Transmission Efficiency by Synaptic Failures. Neural Computation 2004, 16 (6), 1137–1162 DOI: 10.1162/089976604773717568

99. Maass, W.; Natschläger, T. A Model for Fast Analog Computation Based on Unreliable Synapses. Neural computation 2000, 12(7), 1679-1704. DOI: 10.1162/089976600300015303

100. Zott, B.; Simon, M. M.; Hong, W.; Unger, F.; Chen-Engerer, H.-J.; Frosch, M. P.; Sakmann, B.; Walsh, D. M.; Konnerth, A. A vicious cycle of β amyloid–dependent neuronal hyperactivation. Science 2019, 365 (6453), 559–565 DOI: 10.1126/science.aay0198.

101. Busche, M. A.; Konnerth, A. Neuronal hyperactivity - A key defect in Alzheimer's disease? BioEssays 2015, 37 (6), 624–632 DOI: 10.1002/bies.201500004.

102. Atluri, P. P.; Regehr, W. G. Delayed Release of Neurotransmitter from Cerebellar Granule Cells. The Journal of Neuroscience 1998, 18 (20), 8214–8227 DOI: 10.1523/jneurosci.18-20-08214.1998.

103. Lu, T.; Trussell, L. O. Inhibitory Transmission Mediated by Asynchronous Transmitter Release. Neuron 2000, 26 (3), 683–694 DOI: 10.1016/s0896-6273(00)81204-0.

104. Pijnenburg, Y. A. L.; Vd Made, Y.; Van Cappellen Van Walsum, A. M.; Knol, D. L.; Scheltens, P.; Stam, C. J. EEG synchronization likelihood in mild cognitive impairment and Alzheimer's disease during a working memory task. Clinical Neurophysiology 2004, 115 (6), 1332–1339 DOI: 10.1016/j.clinph.2003.12.029.

105. Grady, C. L.; Furey, M. L.; Pietrini, P.; Horwitz, B.; Rapoport, S. I. Altered brain functional connectivity and impaired short-term memory in Alzheimer's disease. Brain 2001, 124 (4), 739–756 DOI: 10.1093/brain/124.4.739.

106. Snyder, E. M.; Nong, Y.; Almeida, C. G.; Paul, S.; Moran, T.; Choi, E. Y.; Nairn, A. C.; Salter, M. W.; Lombroso, P. J.; Gouras, G. K.; et al. Regulation of NMDA receptor trafficking by amyloid-β. Nature Neuroscience 2005, 8 (8), 1051–1058 DOI: 10.1038/nn1503.

107. Stern, E. A.; Bacskai, B. J.; Hickey, G. A.; Attenello, F. J.; Lombardo, J. A.; Hyman, B. T. Cortical Synaptic Integration In Vivo Is Disrupted by Amyloid-beta Plaques. The Journal of Neuroscience 2004, 24 (19), 4535–4540 DOI: 10.1523/jneurosci.0462-04.2004.

108. Wu, Y.; Whiteus, C.; Xu, C. S.; Hayworth, K. J.; Weinberg, R. J.; Hess, H. F.; De Camilli, P. Contacts between the endoplasmic reticulum and other membranes in neurons. Proceedings of the National Academy of Sciences 2017, 114(24), E4859–E4867. DOI: 10.1073/pnas.1701078114

109. Ringsevjen, H.; Umbach Hansen, H. M.; Hussain, S.; Hvalby, Ø.; Jensen, V.; Walaas, S. I.; Davanger, S. Presynaptic increase in IP3 receptor type 1 concentration in the early phase of hippocampal synaptic plasticity. Brain Research 2019, 1706, 125–134 DOI: 10.1016/j.brainres.2018.10.030.

110. Laude, A. J.; Simpson, A. W. M. Compartmentalized signaling: Ca2+ compartments, microdomains and the many facets of Ca2+ signalling. The FEBS Journal 2009, 276 (7), 1800–1816 DOI: 10.1111/j.1742-4658.2009.06927.x.

111. Harraz, F. O.; Altier, C. STIM1-mediated bidirectional regulation of Ca2+ entry through voltage-gated calcium channels (VGCC) and calcium-release activated channels (CRAC). Frontiers in molecular neuroscience 2014, 8, 43 DOI: 10.3389/fncel.2014.00043.

112. Verkhratsky, A. The endoplasmic reticulum and neuronal calcium signalling. Cell Calcium 2002, 32 (5-6), 393–404 DOI: 10.1016/s0143416002001896.

113. Deng, P.-Y.; Rotman, Z.; Jay; Cho, Y.; Cui, J.; Cavalli, V.; Stanislav; Vitaly. FMRP Regulates Neurotransmitter Release and Synaptic Information Transmission by Modulating Action Potential Duration via BK Channels. Neuron 2013, 77 (4), 696–711 DOI: 10.1016/j.neuron.2012.12.018.

114. Pchitskaya, E.; Popugaeva, E.; Bezprozvanny, I. Calcium signaling and molecular mechanisms underlying neurodegenerative diseases. Cell Calcium 2018, 70, 87–94 DOI: 10.1016/j.ceca.2017.06.008.

115. Fujii, S.; Matsumoto, M.; Igarashi, K.; Kato, H.; Mikoshiba, K. Synaptic Plasticity in Hippocampal CA1 Neurons of Mice Lacking Type 1 Inositol-1,4,5-Trisphosphate Receptors. Learning & Memory 2000, 7 (5), 312–320 DOI: 10.1101/lm.34100.

116. Nishiyama, M.; Hong, K.; Mikoshiba, K.; Poo, M.-M.; Kato, K. Calcium stores regulate the polarity and input specificity of synaptic modification. Nature 2000, 408 (6812), 584–588 DOI: 10.1038/35046067.

117. Ito, E.; Oka, K.; Etcheberrigaray, R.; Nelson, T. J.; Mcphie, D. L.; Tofel-Grehl, B.; Gibson, G. E.; Alkon, D. L. Internal Ca2+ mobilization is altered in fibroblasts from patients with Alzheimer disease. Proceedings of the National Academy of Sciences 1994, 91 (2), 534–538 DOI: 10.1073/pnas.91.2.534.

118. Popugaeva, E.; Bezprozvanny, I. Role of endoplasmic reticulum Ca2+ signaling in the pathogenesis of Alzheimer disease. Frontiers in Molecular Neuroscience 2013, 6 DOI: 10.3389/fnmol.2013.00029.

119. Popugaeva, E.; Pchitskaya, E.; Bezprozvanny, I. Dysregulation of Intracellular Calcium Signaling in Alzheimer's Disease. Antioxidants & Redox Signaling 2018, 29 (12), 1176–1188 DOI: 10.1089/ars.2018.7506.

120. Hisatsune, C.; Mikoshiba, K. IP3receptor mutations and brain diseases in human and rodents. Journal of Neurochemistry 2017, 141 (6), 790–807 DOI: 10.1111/jnc.13991.

121. Hanse, E.; Gustafsson, B. Paired-Pulse Plasticity at the Single Release Site Level: An Experimental and Computational Study. The Journal of Neuroscience 2001, 21 (21), 8362–8369 DOI: 10.1523/jneurosci.21-21-08362.2001

122. Bacaj, T.; Wu, D.; Yang, X.; Morishita, W.; Zhou, P.; Xu, W.; Robert; Thomas. Synaptotagmin-1 and Synaptotagmin-7 Trigger Synchronous and Asynchronous Phases of Neurotransmitter Release. Neuron 2013, 80 (4), 947–959 DOI: 10.1016/j.neuron.2013.10.026.

123. Wen, H.; Linhoff, M. W.; Mcginley, M. J.; Li, G.-L.; Corson, G. M.; Mandel, G.; & Brehm, P. Distinct roles for two synaptotagmin isoforms in synchronous and asynchronous transmitter release at zebrafish neuromuscular junction. Proceedings of the National Academy of Sciences 2010, 107(31), 13906–13911. DOI: 10.1073/pnas.1008598107

124. Yang, H.; Xu-Friedman, M. A. Developmental Mechanisms for Suppressing the Effects of Delayed Release at the Endbulb of Held. The Journal of Neuroscience 2010, 30 (34), 11466–11475 DOI: 10.1523/jneurosci.2300-10.2010.

125. Otsu, Y.; Shahrezaei, V.; Li, B.; Raymond, L. A.; Delaney, K. R.; Murphy, T. H. Competition between Phasic and Asynchronous Release for Recovered Synaptic Vesicles at Developing Hippocampal Autaptic Synapses. The Journal of Neuroscience 2004, 24 (2), 420–433 DOI: 10.1523/jneurosci.4452-03.2004.

126. Maximov, A.; Südhof, T. C. Autonomous Function of Synaptotagmin 1 in Triggering Synchronous Release Independent of Asynchronous Release. Neuron 2005, 48 (4), 547–554 DOI: 10.1016/j.neuron.2005.09.006.

127. Wu, L.; Saggau, P. Pharmacological identification of two types of presynaptic voltage- dependent calcium channels at CA3-CA1 synapses of the hippocampus. The Journal of Neuroscience 1994, 14 (9), 5613–5622 DOI: 10.1523/jneurosci.14-09-05613.1994.

128. Mochida, S.; Westenbroek, R. E.; Yokoyama, C. T.; Zhong, H.; Myers, S. J.; Scheuer, T.; Itoh, K.; Catterall, W. A. Requirement for the synaptic protein interaction site for reconstitution of synaptic transmission by P/Q-type calcium channels. Proceedings of the National Academy of Sciences 2003, 100(5), 2819–2824. DOI: 10.1073/pnas.262787699

129. Kaeser, P. S.; Deng, L.; Wang, Y.; Dulubova, I.; Liu, X.; Rizo, J.; Südhof, T. C. RIM Proteins Tether Ca2+ Channels to Presynaptic Active Zones via a Direct PDZ-Domain Interaction. Cell 2011, 144 (2), 282–295 DOI: 10.1016/j.cell.2010.12.029.

130. Keizer, J.; Levine, L. Ryanodine receptor adaptation and Ca2+-induced Ca2+ release-dependent Ca2+ oscillations. Biophysical Journal 1996, 71 (6), 3477–3487 DOI: 10.1016/s0006-3495(96)79543-7.

131. Wu, B.; Yamaguchi, H.; Lai, F. A.; Shen, J. Presenilins regulate calcium homeostasis and presynaptic function via ryanodine receptors in hippocampal neurons. Proceedings of the National Academy of Sciences 2013, 110(37), 15091–15096. DOI: 10.1073/pnas.1304171110

132. Johenning, F. W.; Theis, A.-K.; Pannasch, U.; Rückl, M.; Rüdiger, S.; Schmitz, D. Ryanodine Receptor Activation Induces Long-Term Plasticity of Spine Calcium Dynamics. PLOS Biology 2015, 13 (6), e1002181 DOI: 10.1371/journal.pbio.1002181.

133. Arias-Cavieres A. et al. Ryanodine Receptor-Mediated Calcium Release Has a Key Role in Hippocampal LTD Induction. Frontiers in cellular neuroscience 2018, 12. 403 DOI: 10.3389/fncel.2018.00403

134. Tu, H.; Nelson, O.; Bezprozvanny, A.; Wang, Z.; Lee, S.-F.; Hao, Y.-H.; Serneels, L.; De Strooper, B.; Yu, G.; Bezprozvanny, I. Presenilins Form ER Ca^{2+} Leak Channels, a Function Disrupted by Familial Alzheimer's Disease-Linked Mutations. Cell 2006, 126 (5), 981–993 DOI: 10.1016/j.cell.2006.06.059.

135. Cai, Q.; Tammineni, P. Mitochondrial Aspects of Synaptic Dysfunction in Alzheimer's Disease. Journal of Alzheimer's Disease 2017, 57 (4), 1087–1103 DOI: 10.3233/jad-160726.

136. Du, H.; Guo, L.; Yan, S.; Sosunov, A. A.; Mckhann, G. M. Shidu Yan, S. Early deficits in synaptic mitochondria in an Alzheimer's disease mouse model. Proceedings of the National Academy of Sciences 2010, 107 (43), 18670–18675 DOI: 10.1073/pnas.1006586107

137. Jackson, J.; Jambrina, E.; Li, J.; Marston, H.; Menzies, F.; Phillips, K.; Gilmour, G.; Targeting the Synapse in Alzheimer's Disease. Front. Neurosci. 2019, 735 (13), doi: 10.3389/fnins.2019.00735